Slenderness Limit for Glass Fiber-Reinforced Polymer Reinforced Concrete Columns: Reliability-Based Approach

Koosha Khorramian, Pedram Sadeghian, and Fadi Oudah

ABSTRACT

The slenderness limits in ACI 318 and ACI 440 are based on a deterministic method of defining slender columns as columns whose second-order capacity is lower than 5% of their first-order capacity. For the first time, a reliability-based methodology is developed and employed in this research to quantify the safety associated with existing expressions used to calculate the slenderness limit of concrete columns reinforced with glass fiber reinforced polymer (GFRP) bars, and to propose alternative reliability-based expressions to optimize the design based a predefined target reliability index. The method involves developing a novel artificial neural network (ANN) to conduct second-order analysis, conducting Monte Carlo simulation, and first-order reliability. Analysis results indicate a reliability index ranging from 3.99 to 4.53 for the existing expression in ACI 440. Four alternative design equations for calculating the slenderness limits were proposed and optimized to achieve a target reliability index ranging from 4.0 to 4.5.

DOI: https://doi.org/10.14359/51734495

KEYWORDS

Slenderness Limit, Reliability Analysis, Artificial Neural Network, Concrete Columns, GFRP Bars.

BIOGRAPHICAL SKETCH OF AUTHORS

ACI member **Koosha Khorramian** is a Postdoctoral Fellow in the Department of Civil and Resource Engineering at Dalhousie University, Halifax, NS, Canada, where he also received his Ph.D. in Structural Engineering. He received his M.Sc. and B.Sc. in Structural Engineering from

Sharif University of Technology and Qazvin Azad University, respectively. His research interests include FRP applications for the construction and rehabilitation of concrete structures, steel-concrete composite structures, structural reliability, and AI applications in structural engineering.

ACI member **Pedram Sadeghian** is an Associate Professor and Canada Research Chair in Sustainable Infrastructure in the Department of Civil and Resource Engineering at Dalhousie University, Halifax, NS, Canada. He is an associate member of ACI committee 440 and a voting member of the subcommittees 440-0H (FRP-Reinforced Concrete), 440-0F (FRP-Repair-Strengthening), and 440-0J (FRP Stay-in-Place Forms). His research includes the application of advanced materials and innovative technologies to increase the sustainability of existing and new infrastructure.

ACI member **Fadi Oudah** is an Assistant Professor in the Department of Civil and Resource Engineering at Dalhousie University, Halifax, Nova Scotia, Canada. He is a voting member of ACI Committee 251 (Fatigue of Concrete), ACI Committee 440-0J (FRP Stay-in-Place Forms), and the Standing Committee on Structural Design (SC-SD) of the National Building Code of Canada. His research interests include assessment and retrofit of buildings and bridges using structural reliability, advanced composites, and smart materials.

INTRODUCTION

Fiber-reinforced polymer (FRP) bars have been recognized as an ideal replacement for steel rebar in reinforced concrete (RC) structures in several applications due to their high corrosion resistance, high tensile strength, and ease of installation among other features. Glass FRP (GFRP) bars have gained special attention from the industry because of their relatively lower cost in comparison to carbon FRP (CFRP) bars. For flexural concrete members, such as girders, beams, bridge decks, and slabs, GFRP bars have earned their place in the construction market. However, the market for

GFRP reinforced concrete (GFRP-RC) columns was not flourished due to a lack of convincing evidence on the structural safety of GFRP-RC columns. To address this issue, there have been extensive experimental programs and numerous theoretical studies to investigate the behavior of GFRP-RC columns in recent years [1-10]. Design guidelines and specifications are being developed to consider the recent advancement in GFRP-RC column behavior research and to address the need for considering GFRP as an acceptable solution in the design and construction industries.

Optimizing the design of GFRP-RC columns by balancing the cost-to-safety is required to promote their application in industry, especially the slenderness limit set by design standards. The slenderness limit is defined as the ratio of the effective length to the gyration radius of a column where the secondary moment effects cannot be ignored for columns with ratios greater than the limit. In other words, columns whose slenderness ratio is greater than the slenderness limit, named slender columns, require a second-order analysis to determine their capacity, while columns with lower slenderness ratios are considered as short columns and designed using a first-order analysis. To achieve the balance between the safety and economy of the design, the safety corresponding to the slenderness limit should be quantified and set to an acceptable target reliability index. Review of relevant literature indicates that the slenderness limits in design codes are not reliability-based, hence, a research gap related to quantifying the safety of these limits exists.

The criterion of determining the slenderness limit of steel-RC columns was set by MacGregor et al. in 1970 [11]. This criterion sets the slenderness limit in such a way that the majority of columns whose second-order capacity is lower than 5% of their first-order capacity are considered slender columns. MacGregor et al. [11] proposed an equation for the slenderness limit

of steel-RC columns for sway and non-sway frames which was adopted by ACI 318-19 [12], as follows:

$$\lambda_{cr} = 34 + 12\left(\frac{M_1}{M_2}\right) \leq 40 \quad (1)$$

where λ_{cr} is the slenderness limit, M_1 and M_2 are the smaller and larger end moments for a column, and M_1/M_2 is the moment ratio which is negative for single curvature and positive for double curvature. Eq. (1) is a simplified linear equation with a constant cap that passes through the actual data points from an analysis for which the axial capacity was calculated by setting a 5% drop for the second-order to the first-order analysis. The cap of 40 was assumed for the slenderness limit in Eq. (1) which is corresponding to a moment ratio of 0.5 (i.e., M_1/M_2=0.5) where one end moment is minus half of the other end moment [11], as presented in Fig. 1.

The differences in material properties, modes of failure, and the resistance model for GFRP-RC columns compared to steel-RC columns, revealed a need for studies on GFRP-RC columns. In addition, the lower modulus of elasticity of GFRP bars in comparison to steel bars is likely to result in higher secondary moment effects for GFRP-RC columns in comparison to steel-RC columns. Therefore, there was a need to investigate the slenderness limit of GFRP-RC columns.

Mirmiran et al. [13] reported the first study on the determination of slenderness limit for concrete columns reinforced with FRP bars (referred to as FRP-RC columns in this study). In the study, a numerical and statistical approach was adopted, and a slenderness limit of 17 was proposed for GFRP-RC columns in sway frames. In 2013, Zadeh and Nanni [14] suggested shifting Eq. (1) so that the slenderness limit equation starts with the slenderness ratio of 17 for GFRP-RC columns, proposed by Mirmiran et al. [13], as presented in Fig. 1. As a result of shifting 22 to 17 for the

symmetric single curvature case, for double curvature cap, the same shift changed the cap of 40 to 35, as presented in Eq. (2).

$$\lambda_{cr} = 29 + 12\left(\frac{M_1}{M_2}\right) \leq 35 \quad (2)$$

The latter equation (i.e., Eq.2) is being adopted for the ACI 440 code accompanied to ACI 318-19 [12], with a conservative cap of 30 instead of cap of 35 in Eq. 2 (which was chosen based on ACI 440 committee decision) for the slenderness limit as presented in Eq. (3).

$$\lambda_{cr} = 29 + 12\left(\frac{M_1}{M_2}\right) \leq 30 \quad (3)$$

In 2017, Zadeh and Nanni [15] used an analytical approach and proposed a slenderness limit corresponding to a 5% drop or equal to a moment magnification factor of 1.14 for GFRP-RC columns at high levels of axial loads in the interaction diagram (i.e., low eccentricity) by utilizing simplified assumptions, as presented in Eq. (4).

$$\lambda_{cr} = 28 + 14\left(\frac{M_1}{M_2}\right) \leq 35 \quad (4)$$

Also, the latter study [15] recommended lower slenderness limits for high-strength concrete columns reinforced with FRP bars and corresponding modification factors for high-strength concrete. Zadeh and Nanni [15] proposed a cap of 31 as the slenderness limit of GFRP-RC columns for a concrete strength of 70 MPa, which might be related to the selection of the cap of 30 in Eq. 3 by ACI 440 committee.

In 2020, Abdelazim et al. [16] proposed a slenderness limit of 18 for sway frames and its corresponding formulation for non-sway frames for FRP-RC columns based on an experimental database and an analytical approach with the 5% drop criterion, and by shifting Eq. (1) to start from the slenderness limit of 18 for the symmetric single curvature case, as presented in Eq. (5).

$$\lambda_{cr} = 30 + 12\left(\frac{M_1}{M_2}\right) \leq 36 \quad (5)$$

While the 5% drop criterion is accepted and vastly used in the design guidelines, the safety associated with slenderness limits found using the 5% drop approach has not been quantified. Therefore, the objectives of this study are to: 1) propose a generic method for quantifying the reliability index (β) corresponding to the slenderness limit; 2) apply the method to GFRP-RC columns to evaluate the reliability index corresponding to the slenderness equation proposed in ACI 440 design code accompanied to ACI 318-19 [12]; and 3) provide recommendations for slenderness limit equation for GFRP-RC columns.

The proposed method in this study has three features: 1) reliability-based approach using Monte Carlo simulation (MCS), first-order reliability method (FORM) modified by Rackwitz and Fiessler (FORM-RF) using 10,497,600 different column cases; 2) artificial neural network (ANN) modeling of slender GFRP-RC columns trained by 5,832,000 different analyses using finite-difference method (FDM) to cover 12 design parameters; 3) utilizing experimental database for GFRP-RC columns in the reliability analysis. The load and resistance models which include the ANN modeling are discussed first, followed by detailing the reliability method, and continued with a parametric study, code evaluation, and design recommendations to conclude the study.

RESEARCH SIGNIFICANCE

There exists a general need for global optimization of slenderness limit for GFRP-RC columns to balance the safety-to-cost ratio. For design purposes, a high slenderness limit results in less reliable designs, and a low slenderness limit leads to overdesigned columns. In this study, for the first time, a novel reliability-based approach was adopted to quantify the safety associated with the slenderness limit of GFRP-RC columns. The application of this approach reflects in the development of design specifications for the design of GFRP-RC columns, such as the ACI 440 code, and impacts the economic aspects of the design industry.

ANALYSIS FRAMEWORK

The methodology consists of a reliability-based analysis that relates the first-order and second-order axial capacity of RC columns to the loads and resistance distribution. In the following, the load and resistance models are established to perform a reliability analysis on a design space containing 10,497,600 different cases using a combination of 12 design parameters. The analysis combines Monte Carlo simulation (MCS) and first-order reliability method (FORM) which considers the distribution types of the input design parameters (i.e., the Rackwitz and Fiessler variation of the FORM [17, 18] or FORM-RF). The established methodology is general and can be used for different design codes.

Resistance Model

The resistance model should reflect the real capacity of a concrete column. Experimental testing is the best source to quantify the resistance of a column. However, even for a single column with known nominal design parameters, due to the variable nature of the constituent materials, geometry, and simplified assumptions, a large group of tested specimens are required to build the resistance distribution. Considering a thorough study with a large number of cases to cover multiple variations of different parameters, the experimental resistance can be replaced by numerical models to increase the efficiency of the calculation. Meanwhile, the accuracy of the ratio of numerical to experimental models can be considered as a random variable whose effect can be considered in the reliability analysis. In this study, the base of the resistance model is the finite difference method (FDM) which showed a good degree of accuracy for modeling concrete columns reinforced with GFRP bars, steel rebar, CFRP strips, GFRP wraps, CFRP wraps, or any combination of this internal and external reinforcement [19].

The basic idea of FDM is to divide the column into n nodes to have n-1 column elements and solve the differential equation of the column to find the desired response of the column. Fig.

2(a) shows the schematic FDM model where e_1 and e_2 are the eccentricities at the top and bottom of the column, P is the axial applied compressive load, b and h are width and height of the column cross-section, and ρ is the reinforcement ratio. The moment diagram for the column shown in Fig. 2(a) is presented in Fig. 2(b) where M_1 and M_2 are the end moments due to the eccentric loading. The model is able to assess single and double-curvature deflection shapes. The boundary condition dictates a zero displacement at both ends of the column (i.e., simply supported column).

The analysis starts with the evaluation of the displacement corresponding to a certain load level by using the discrete form of the differential equation of the columns for each element, satisfying the equilibrium at each point of the column, and satisfying the boundary condition. The material nonlinearity including concrete and reinforcement reflects in the moment-curvature diagram corresponding to each load level that can be found using an iterative section analysis, as presented in Fig. 2(c). Section analysis assumes a linear strain profile with a perfect bond between the reinforcement and concrete. The nonlinear concrete material model suggested by Popovics [20] was used for concrete in compression while the tensile strength of the concrete was neglected. The GFRP material is considered linear elastic up to crushing in compression or rupture in tension. The steel material was considered as a bilinear elastic perfectly plastic.

The displacement corresponding to the certain load level can be found using the iterative procedure, as explained, and shown in Fig. 2(c). By examining different load levels with a proper algorithm, the ascending branch, peak load, and the descending branch for post-peak behavior can be obtained. Further information on implementation and details of the FDM modeling for different columns can be found in the literature [19, 21- 24]. It should be noted that since the material nonlinearity for concrete, crushing and rupture of GFRP bars, and global buckling are considered

in the FDM model, the brittleness of material and slenderness effects are implicitly considered in the reliability analysis.

The FDM was validated for GFRP-RC columns and steel-RC columns with a database of 85 GFRP-RC and 102 steel-RC tests collected from fourteen independent studies in the literature [2, 9-10, 25-35]. The database for GFRP-RC and steel-RC tests are available in Appendix-1 and Appendix-2, respectively. The results of the theoretical (i.e., FDM analysis) versus experimental tests for GFRP-RC columns and steel-RC columns are presented in Fig. 3(a) and 3(b), respectively. Also, the corresponding histograms of the theoretical (i.e., FDM analysis) to experimental ratio (ψ_{TE}) for GFRP-RC columns and steel-RC columns are shown in Fig. 3(c) and Fig. 3(d), respectively. The results showed good accuracy with a mean (μ), standard deviation (σ), and a coefficient of variation (CoV) of 1.10, 0.15, and 0.14, respectively, for GFRP-RC columns, and 1.04, 0.11, and 0.10, respectively, for steel-RC columns. The distribution for ψ_{TE} for both GFRP-RC and steel-RC columns was recognized as a lognormal distribution. These ratios are considered as random variables in the reliability analysis to account for the variance in the analysis method.

The FDM analysis with ψ_{TE} represents the resistance defined as the second-order axial capacity found by FDM divided by ψ_{TE}. Conducting a comprehensive case study using the FDM model requires significant computational power and takes extraordinary time to complete. For example, calculating the reliability indexes for about 10 million cases requires approximately 0.25 million days to complete considering a 90-core workstation. Therefore, an alternative and accurate second-order analysis is required to strongly enhance the computation efficiency. In this study, an artificial neural network (ANN) was utilized as a surrogate model to the second-order FDM analysis. By replacing FDM by ANN in the resistance model, the ratio of ANN to theoretical (or FDM) would also be required to modify the resistance model.

The ANN was successfully utilized to conduct reliability analysis for structural elements [36], to evaluate the shear capacity of FRP-RC beams [37], to determine the axial capacity of short GFRP-RC columns [38], and to obtain the reliability of short FRP-RC columns [39]. In the current study, a nonlinear second-order analysis was developed using trained ANN models for slender GFRP-RC and steel-RC columns, for the first time, to be used in the resistance model for the reliability analysis.

The ANN is a nonlinear regression with a substantially larger size of predictor coefficient and deeper connecting of coefficients than the regular regression. Fig. 4 shows an ANN with one input layer, three hidden layers, and one output layer. The neurons are shown as circles and the weights are shown as lines in Fig. 4, while the set of neurons and weights are considered as the network. Except for the neurons in the first layer which are external inputs to the analysis, each neuron in each layer is a function of a linear combination of all neurons times their corresponding weights that enter the neuron from the previous layer plus a specific constant bias value assigned to each neuron. This linear combination is scaled using a function called activation function which assigns a value between zero to one to each neuron, where one is completely active and zero is ineffective in the network. The value of each neuron is represented in Eq. (6) and Eq. (7) [40].

$$a_j^{(k)} = \sigma\left(\sum_{i=1}^{n} w_{ji} a_i^{(k-1)} + b_j^{(k)}\right) \tag{6}$$

$$\sigma(z) \equiv \frac{1}{1+e^{-z}} \tag{7}$$

where $a_j^{(k)}$ is the j^{th} neuron in the k^{th} layer to be evaluated, $a_i^{(k-1)}$ is the neuron in the i^{th} neuron in the $(k\text{-}1)^{th}$ layer previous to layer k, $b_j^{(k)}$ is the bias corresponding to neuron $a_j^{(k)}$, w_{ji} is the weight that connects neuron $a_i^{(k-1)}$ into neuron $a_j^{(k)}$, σ is the Sigmoid activation function, and z is the argument of the sigmoid function.

The predictor of ANN should be trained with a set of input/output data generated with a more precise analysis method (called a computer-based database). The goal of training is to find all weights and biases of the network so that the least squared error of the predicted value and the training database is optimized. In addition to optimizing the trained network finding the optimum configuration of the network is required (i.e., finding the number of hidden layers, activation function, optimization algorithm, etc.).

To achieve the optimized configuration, a sensitivity analysis is required. For the sensitivity analysis, the computer-based database is divided into training and validation datasets. The network is trained with different configurations and each time the root mean squared error (RMSE) of the training and validation sets is evaluated. If the RMSE of training is comparatively high, the prediction is poor and the network is undertrained, and if the RMSE of training is low, but the RMSE of the validation set is high, the network only predicts acceptable values for the training data and is overtrained, which means the response is memorized by the network. Only the network with low RMSE for both training and validation sets is reliable which is called the optimum configuration.

To find the optimized configuration of an ANN for GFRP-RC columns, a total of 5,832,000 FDM models were built with 12 design parameters, as presented in Table 1. In this study, the optimum configuration was found in three phases. In phase I, one, two, and three hidden layers with 3 to 45 neurons in each layer, Sigmoid and rectified linear unit (ReLU) activation functions, and Bayesian regularization and Levenberg-Marquardt backpropagation algorithms were examined using 5% of the whole database. The results show that three hidden layers, the Sigmoid activation function, and the Levenberg-Marquardt backpropagation algorithm led to the optimum configuration. Also, phase I revealed that 35 neurons for the first layer of ANN are appropriate.

Phase II was conducted using 50% of the database by considering 71 different configurations by varying neurons in the second and third layers. Phase II revealed that 30 neurons in the second layer led to the optimum configuration. Finally, in phase III, 100% of the database and two of the best configurations were examined. The results showed that 15 neurons for the third layer are appropriate. It should be mentioned that for all phases, 70% and 30% of the studied database were considered for training and validation, respectively.

The optimum configuration for the second-order analysis of GFRP-RC columns is shown in Fig. 5(a). To compare the reliability results, a second-order ANN was developed for steel-RC columns. The same configuration was used to train the network for second-order analysis of steel-RC columns, except for the number of neurons in the input layer, as presented in Fig. 5(b). For steel-RC columns, only 54,000 FDM analyses were considered with 7 different design parameters. It should be mentioned that the parametric study results in the next section revealed that some of the parameters are ineffective in the reliability analysis, which leads to a reduced number of design parameters for training of the ANN for steel-RC columns.

In this study, three second-order ANN models were developed. A comparison of 2,916,000 different FDM versus ANN analyses was shown in Fig. 6(a) and 6(b), for GFRP-RC columns with a width of 254 mm [10 in.] and 457 mm [18 in.], respectively, and a comparison of 54,000 different FDM versus ANN analysis was shown in Fig. 6(c) for steel-RC columns, where F_{ANN} is second-order axial capacity predicted ANN and F_{theo} is the second-order axial capacity calculated by the theoretical method (i.e., FDM). The results revealed a very good agreement between the FDM and ANN analysis with a coefficient of determination of one (i.e., R^2=1) and RMSE of 1 kN for all three models (where $RMSE = \sqrt{\frac{\sum(F_{ANN}-F_{theo})^2}{N}}$ for N number of studied cases). The ratio of ANN to FDM model (i.e., ψ_{AT}) was determined for GFRP-RC columns with a width of 254 mm [10 in.]

and 457 mm [18 in.], as shown in Fig. 6(d) and 6(e), respectively, and for steel-RC columns with a width of 254 mm [10 in.], as shown in Fig. 6(f). For all three models, ψ_{AT} has a mean value of one and a coefficient of variation of less than 0.15%, as shown in Fig. 6.

The resistance model required for reliability analysis (i.e., *R*) can be built using Eq. (8), by knowing the second-order axial capacity using the ANN model (i.e., P_{2nd}), the distribution of FDM to experimental ratio (i.e., ψ_{TE}), and the distribution of ANN to FDM ratio (i.e., ψ_{AT}).

$$R = \frac{P_{2nd}}{\Psi_{AT}\Psi_{TE}} \tag{8}$$

Design parameters including the concrete strength, depth of bars in tension and compression, the tensile strength of GFRP bars, and compressive strength of GFRP bars, were considered as random variables for GFRP-RC columns, as presented in Table 2. The statistical input parameters were based on the studies used for calibrating the load and resistance factors in ACI 318 and ACI 440 [41, 42]. The bias for concrete strength can be calculated with Eq. (9) [42].

$$k_{fc} = -0.0081f_c^3 + 0.1509f_c^2 - 0.9338f_c + 3.0649 \tag{9}$$

where k_{fc} is the bias for concrete strength and f_c is the concrete strength (in ksi for Eq. (9)). For steel-RC columns, the random variables related to GFRP bars were substituted by the yield stress of the steel rebar. In addition, the FDM to experimental ratio (i.e., ψ_{TE}) was considered as a random variable for both GFRP-RC and steel-RC columns, as presented in Table 2. The ANN to FDM ratio (i.e., ψ_{AT}) was considered as a deterministic value due to its low coefficient of variation.

Load Model

In this study, only the dead and live loads were considered as random variables. The distribution of dead and live loads (i.e., *D* and *L*) are presented in Table 2. For the reliability analysis, several dead-to-live load ratios from 0.25 to 9 were considered, and special cases for only dead and only

live load were also considered in the analysis to cover a range of zero to one for $D/(D+L)$, as presented in Table 3.

Reliability Analysis

The reliability analysis was established based on the probability of failure of a column, where it is designed using first-order analysis but failed by considering secondary moment effects in the resistance. The slenderness limit is the highest slenderness ratio for a column to be considered as a short column, for which the first-order analysis is allowed instead of the second-order analysis of the column. The neglected secondary moment effect leads to a reduced resistance of the columns, and in turn a higher probability of failure. By changing the slenderness limit for different column cases, the corresponding reliability index can be found using the procedure described in this section. Table 3 shows 10,497,600 cases considered for the reliability analysis of GFRP-RC columns using 13 different parameters. For each case, the reliability method illustrated in Fig. 7 was applied to find the reliability index corresponding to each case.

The reliability analysis procedure consists of three parts: 1) obtaining the resistance distribution; 2) obtaining the load distribution; and 3) calculating the reliability index. To find the resistance distributions, a Monte Carlo simulation (MCS) with 1000 trials was performed for each case. The resistance model used in MCS (i.e., Eq. (8)) is a nonlinear second-order analysis that involves the experimental database (with ψ_{TE}). To conduct MCS, the resistance model was evaluated using 1000 randomly generated input sets for the resistance function and using five random variables related to resistance for GFRP-RC columns, as presented in Table 2. At this stage, the mean, standard deviation, and the distribution type for the resistance are found. The distribution of resistance was recognized as lognormal for all cases.

The distribution of the loads is available in the literature [42] for calibrating the load and resistance factors for ACI 318 code, as presented in Table 2. However, the mean value should be

assessed for each case, for which a factored first-order analysis was used. The utilization ratio of the column is set to unity (i.e., ratio of demand-to-capacity) for the ACI 318 load combinations presented in Eq. (10) and Eq. (11) [12].

$$\phi_n P_{1st} = 1.2P_D + 1.6P_L \quad (10)$$

$$\phi_n P_{1st} = 1.4P_D \quad (11)$$

where P_{1st} is the first-order axial capacity found from the interaction diagram of GFRP-RC columns calculated based on ACI 440 code, P_D and P_L are the nominal values for dead and live loads, respectively, and ϕ_n is the resistance reduction factor for GFRP-RC columns. The value of ϕ_n was considered as 0.65 for the rest of the study since GFRP-RC columns tested in the literature only experienced compression-controlled failure because of concrete spalling in the compression side [43]. Eq. (10) requires a dead-to-live load ratio to determine the nominal values of dead and live loads, which is considered in Table 3. The nominal loads are multiplied with their corresponding bias in Table 3 to establish the mean value of the load distributions. The coefficient of variation times the mean of loads yields the standard deviation of the loads. The distribution of considered loads in this study is normal [42].

The first-order reliability method (i.e., FROM-RF) was used to assess the corresponding reliability index by considering the established resistance and load distributions. More details for FROM-RF reliability analysis can be found in the literature [17, 18]. Also, the approach of having an MCS for finding resistance distribution combined with a reliability method to find the reliability index was used by Mirza et al. [44] to calibrate the stiffness reduction factor for ACI 318-83 [45], which validates the methodology. The results of the current study were used to perform a parametric study, and to evaluate slenderness limits.

PARAMETRIC STUDY

To perform a parametric study, the reliability indexes of all cases presented in Table 3 were divided based on the end moment ratio (i.e., M_1/M_2), the proportion of dead load over the total load (i.e., $D/(D+L)$), and the slenderness limit (i.e., λ_{cr}). For each design parameter, the reliability indexes of all cases that share the same design parameter were averaged. The results of the parametric study revealed that only five parameters are effective including the concrete strength (i.e., f_c), eccentricity ratio (i.e., e/h), reinforcement depth ratio (i.e., γ), reinforcement ratio (i.e., ρ), and to a very low extent the modulus of elasticity of GFRP bars (i.e., E_{frp}). The reliability indexes can be solely found using only the effective parameters shown as the reduced cases in Table 3, which include 97,000 cases. The remaining parameters were ineffective in the reliability index calculation (i.e., the reliability index is insensitive to variation in the parameter value).

The ineffective parameters included the shape of the cross-section (square and rectangular with aspect ratios ranging from 0.75 to 1.25) and the rebar layout (two sides and four sides). The analysis results are believed to be also appliable for the circular sections since the insensitivity of the reliability index to variations in the section aspect ratio and rebar layout for the considered square and rectangular sections is indicative that the section shape is, generally, not an effective parameter and it is unlikely for a circular section with similar material properties as those considered in this study to influence this observation.

The results of the parametric study for GFRP-RC columns are shown in Fig. 8, where the reliability index is shown as β, and slenderness limit is shown as λ_{cr}. The results revealed that as concrete strength increases, the reliability index decreases (Fig. 8(a)) because the mean value for loads increases, which is determined by first-order analysis. The resistance also increases by increasing the concrete strength due to the higher strength and stiffness of the column, but the load

increase is more effective since the utilization ratio of one dictates that the factored loads are equal to the factored capacity. As an example, for $D/(D+L)$ ratio of 0.8, a slenderness ratio of 17, and M_1/M_2 ratio of -1, as concrete strength increases from 20 to 40 and 60, the reliability index decreases from 4.59 to 3.89 and 3.50, respectively. Considerations along the same direction can be found in the slenderness limit suggested by CSA A23.3 [46], and Zadeh and Nanni [15], where the slenderness limit is reduced for higher concrete strengths.

For the eccentricity ratio, two trends were observed based on the end moment ratio (i.e., M_1/M_2). For single curvature cases (i.e., M_1/M_2=-1), as the eccentricity ratio increases, the reliability index decreases since the resistance decreases due to higher flexural loads for single curvature columns (Fig. 8(b)). For example, for a $D/(D+L)$ of 0.8 and a slenderness ratio of 17, as the eccentricity ratio increases from 0.1 to 0.3 and 0.5, the reliability index decreases from 4.05 to 4.00 and 3.92, respectively. However, for end moment ratios other than -1, as eccentricity increases, the reliability index increases (Fig. 8(b)). For example, for a $D/(D+L)$ of 0.8 and a slenderness ratio of 17, as the eccentricity ratio increases from 0.1 to 0.3 and 0.5, the reliability index increases from 4.26 to 4.58 and 4.81, respectively. This is because the effective length is higher and the decrease in the resistance of the column due to higher eccentricities have a dominant effect for the single curvature cases. However, for end moment ratios other than -1, the increase in the eccentricity has less effect on reducing the resistance, and the increase in the mean value of the axial loads for end moment ratios other than -1, is higher than single curvature since the larger end moment (i.e., M_2) controls the first-order analysis and the mean of loads. For the reinforcement depth ratio, reinforcement ratio, and modulus of elasticity of GFRP bars, the results showed that the reliability indexes decrease as the value of the considered parameter increases since the resistance decrease has a dominant effect by increasing these parameters.

For comparison purposes, the analysis procedure was applied to steel-RC columns using the effective parameters as presented in Table 3. The first-order analysis required for the determination of the mean of loads was adjusted for steel-RC columns using ACI 318-19 [12], and the statistics for yield stress are added, as presented in Table 2. The results of the parametric study for steel-RC columns are shown in Fig. 9. For steel-RC columns, similar behavior of reliability index for various parameters was observed to the results for GFRP-RC columns. However, the effects of the reinforcement ratio and reinforcement depth are higher in the steel-RC column reliability analysis as the yielding of steel affects the analysis.

The reliability results for GFRP-RC and steel-RC columns are presented in Fig. 10(a) and 10(b), respectively. Overall, the reliability index of steel-RC columns is higher than GFRP-RC columns for all cases because of the difference in the material properties, failure behavior, and statistics. For example, for a single curvature case with $D/(D+L)$ of 0.8, for slenderness ratios of 17 and 22, the reliability indexes for steel-RC columns were 4.79 and 4.65, respectively, while for GFRP-RC columns the corresponding reliability indexes were 3.99 and 3.82, respectively. For all cases, it was observed that as the end moment ratio varies from single curvature (i.e., $M_1/M_2 = -1$) to double curvature (i.e., $M_1/M_2 = 1$), the reliability index increases. The latter can be explained by the fact that for the design of a column with different end moments, the larger end moment governs the first-order analysis, which in turn results in smaller axial factored capacity for double curvature compared to single curvature columns. Thus, the mean value of the load for double curvature cases is lower than the ones found for single curvature cases. At the same time, when different end moments exist, the effective length of the column is reduced, which causes higher resistance. Therefore, by moving from single to double curvature cases, the reliability index increases. For example, for $D/(D+L)$ of 0.8, and slenderness ratio of 17, the reliability index increases from 3.99

to 4.55 by moving from single curvature to double curvature case for GFRP-RC columns. The latter is compatible with the suggestions for slenderness limit in ACI 318-19 [12], ACI 440, and CSA A23.3 [46], where a higher slenderness limit can be considered for cases with different end-moment ratios. Also, for all cases, the results of the reliability analysis revealed that as the slenderness ratio increases the reliability index decreases since the resistance is affected more by the secondary moment effects.

CODE EVALUATION AND RECOMMENDATIONS

In this section, the reliability indexes found in this study were used to evaluate the slenderness limit equations available in the literature and design codes. A dead-to-live load ratio of 4 was considered since it makes the worst effect based on the findings of a recent survey [47]. It should be noted that this value is higher than the usual live-to-dead load ratio used for the calibration of resistance factors for GFRP-RC columns [41] and found based on actual measurements of office loads [47].

The reliability of the slenderness limits is expressed in Eqs. (1) to (5) is presented in Fig. 11. The proposed slenderness limit for GFRP-RC columns to be included in ACI 440, which is a combination of proposed slenderness limits by Mirmiran et al. [13] and Zadeh and Nanni [14], is presented in Fig. 11(a). The results showed a range of 3.99 to 4.53 for the reliability index which almost meets the acceptable target reliability index of 4.0 for RC columns set by Szerszen and Nowak [48] for the calibration of the member reduction factors in ACI 318. For comparison, the reliability index corresponding to the slenderness limit in ACI 318-19 [12] is presented in Fig. 11(b), which shows higher reliability indexes for steel-RC columns (starting from a reliability index of 4.65) compared to GFRP-RC columns. Comparing the ACI 318-19 slenderness limit with the target reliability index of 4.0, it can be concluded that the equation is conservatively selected.

The reliability index evaluation for the proposed slenderness equations by Zadeh and Nanni [15] and Abdelazim et al. [16] are presented in Fig. 11(c) and 11(d), respectively. The results revealed that all reliability indexes are higher than the target reliability index of 4.0 except the slenderness ratio of 18 which is slightly lower than the target reliability.

The slenderness limit cap for GFRP-RC columns in the existing expressions of the slenderness limit was a result of shifting the cap of 40 for steel-RC columns, in ACI 318-19 [12], as explained in the introduction section. Reliability analysis shows that the cap for the slenderness limit is conservatively selected in the existing expressions, and the reliability indexes for the cap are higher than the target reliability index of 4.0 for columns.

To optimize the slenderness limit equation, a slenderness limit cap of 40, based on ACI 318-19 [12], and a similar slope as Eq. (1) were used to develop a new slenderness limit equation that starts with the target reliability of 4.0 for columns. The results showed that a slenderness limit of 16.5 corresponds to the target reliability of 4.0. Therefore, Eq. (12) is proposed to be used for GFRP-RC columns in this study, as presented in Fig. 12(a).

$$\lambda_{cr} = 28.5 + 12\left(\frac{M_1}{M_2}\right) \leq 40 \tag{12}$$

where λ_{cr} is the slenderness limit, M_1 and M_2 are the smaller and larger end moments for a column, and M_1/M_2 is the moment ratio which is negative for single curvature and positive for double curvature. To further optimize Eq. (12), by keeping the boundaries of 16.5 and 40 for end moment ratios of 1 and -1, respectively, and adding a condition of zero slopes at the slenderness limit of 40, a quadratic slenderness limit equation is also proposed in this study, presented in Eq. (13) and Fig. 12(a).

$$\lambda_{cr} = 34\frac{1}{8} + 11\frac{3}{4}\left(\frac{M_1}{M_2}\right) - 5\frac{7}{8}\left(\frac{M_1}{M_2}\right)^2 \tag{13}$$

One step further in optimizing the slenderness limit equation is to find the upper limit of 4.5 for the target reliability of columns [48] for the double curvature case. It should be noted that a target of 4.0 could have been selected to optimize the upper limit, which would lead to an impractical and high slenderness limit. The investigation showed that a slenderness limit of 57 corresponds to a target reliability index of 4.5 for GFRP-RC columns. By changing the cap from 40 to 57 for double curvature and keeping the slenderness limit of 16 for the symmetric single curvature case, linear and quadratic optimized equations for slenderness limit of GFRP-RC columns are presented in Eq. (14) and Eq. (15), respectively, as shown in Fig. 12(b).

$$\lambda_{cr} = 36\frac{3}{4} + 20\frac{1}{4}\left(\frac{M_1}{M_2}\right) \tag{14}$$

$$\lambda_{cr} = 46\frac{7}{8} + 20\frac{1}{4}\left(\frac{M_1}{M_2}\right) - 10\frac{1}{8}\left(\frac{M_1}{M_2}\right)^2 \tag{15}$$

For design recommendation, Eq. (12) or Eq. (15) are recommended for design codes. Eq. (12) utilizes the traditional simple linear format of slenderness limit in ACI 318 and ACI 440 but yields a further optimized slenderness limit as compared with the existing ACI expressions. Eq. (15) represents the most optimized expression for the slenderness limit due to the quadratic power used for the expression, the increase in the cap from 35 to 40, and the decrease in the single curvature slenderness limit from 17 to 16.5 to meet a target reliability index of 4.0.

FUTURE STUDIES

The reliability approach introduced in this paper is generic and can be further utilized for quantifying the safety margin of Load and Resistance Factor Design (LRFD) based design codes, and for different columns such as FRP-wrapped concrete columns, concrete-filled FRP tubes (CFFTs), and hybrid RC columns. The study can be expanded to cover high strength and ultra-high-strength concrete columns reinforced with GFRP bars provided that an adequate database can be developed. The effect of creep was not considered in this study although it can be considered

in future studies for completeness purposes. The analysis results presented in this work are based on columns in non-sway frames. Future research can be conducted to examine the sensitivity of the analysis findings to columns in sway frames subjected to lateral loads (wind and earthquake).

CONCLUSION

A new methodology for quantifying the reliability index of slenderness limit is proposed for the first time, with which the reliability of GFRP-RC columns was assessed. As a part of the resistance model development, a novel second-order analysis for GFRP-RC columns was developed using an optimized ANN trained by 5,832,000 nonlinear FDM analyses. The optimized configuration was found in three phases which have a sigmoid activation function, Levenberg-Marquardt backpropagation algorithm, and three hidden layers with 35, 30, and 15 neurons in the first, second, and third layers, respectively. A parametric study with 10,497,600 column cases for a design space built with 12 different design parameters for GFRP-RC columns was conducted to calculate the reliability indexes. The following conclusions are drawn from this study:

- The results of the parametric study showed that the concrete strength, eccentricity ratio, reinforcement ratio, reinforcement depth ratio, and modulus of elasticity of GFRP bars had pronounced effects in the reliability index calculation out of twelve studied parameters.
- Concrete strength and eccentricity ratio were the most effective parameters. For a $D/(D+L)$ of 0.8 and a slenderness ratio of 17, as concrete strength increases from 20 to 60, the reliability index decreases from 4.59 to 3.50. For the same $D/(D+L)$ and slenderness ratio, as the eccentricity ratio increases from 0.1 to 0.5, the reliability index decreases from 4.05 to 3.92 for single curvature case, and the reliability index increases from 4.26 to 4.81 for double curvature case.

- The results showed that as the slenderness limit increases, the reliability index decreases. For GFRP-RC columns with a $D/(D+L)$ of 0.8 and a single curvature case, as the slenderness ratio increases from 14 to 40, the reliability index drops from 4.08 to 2.76.
- The results indicated the increase in the reliability index as the end moment ratio varies from single curvature to double curvature. For $D/(D+L)$ of 0.8, and slenderness ratio of 17, the reliability index increases from 3.99 to 4.55 by moving from single curvature to double curvature for GFRP-RC columns.
- The methodology was applied to steel-RC columns and similar behavior was observed, but with higher reliability indexes in comparison to GFRP-RC columns.
- The slenderness limit equations proposed in the literature and the proposed equation for ACI 440 code for GFRP-RC columns, and the slenderness limit in ACI 318-19 for steel-RC columns were evaluated. The results showed that most of the proposed equations meet the target reliability of 4.0 for concrete column calibration of ACI codes. The equations were conservatively selected.
- To optimize the slenderness limit, a target reliability range of 4.0 to 4.5 was selected. Four new equations were proposed for the slenderness limit of GFRP-RC columns (i.e., Eq. (12) to Eq. (15)). The reliability index of 4.0 corresponds to a slenderness limit of 16.5 for symmetric single curvature cases, while the reliability index of 4.5 corresponds to a slenderness limit of 57 for GFRP-RC columns for the double curvature case.
- Eq. (12) and Eq. (15) are recommended for the design codes. Eq. (12) utilizes the traditional basic linear format of the existing slenderness limit in ACI 318 and ACI 440, but yields a further optimized slenderness limit as compared with the existing ACI expressions, while the quadratic Eq. (15) represents the most optimized expression for the slenderness limit.

- The results of this study are valid in the range of studied parameters. The methodology is generic and can be applied to assess the reliability index corresponding to the slenderness limit for different codes and material properties.

ACKNOWLEDGEMENT

The authors would like to thank Dalhousie University and the Natural Sciences and Engineering Research Council (NSERC) for supporting this research program.

DATA AVAILABILITY

Some or all data, models, or codes generated or used during the study are available from the corresponding author by request.

REFERENCES

1. Barua, S.; Mahmoud, K.; and El-Salakawy, E., "Slender GFRP-RC Circular Columns under Concentric, Eccentric, and Flexural Loads: Experimental Investigation," *Journal of Bridge Engineering*, V. 26, No. 7, 2021, pp. 04021033.

2. Khorramian, K., and Sadeghian, P., "Experimental Investigation of Short and Slender Rectangular Concrete Columns Reinforced with GFRP Bars under Eccentric Axial Loads," *Journal of Composites for Construction*, V. 24, No. 6, 2020, pp. 04020072.

3. Barua, S., and El-Salakawy, E., "Performance of GFRP-Reinforced Concrete Circular Short Columns under Concentric, Eccentric, and Flexural Loads," *Journal of Composites for Construction*, V. 24, No. 5, 2020, pp. 04020044.

4. Abdelazim, W.; Mohamed H. M.; and Benmokrane, B., "Inelastic Second-Order Analysis for Slender GFRP-Reinforced Concrete Columns: Experimental Investigations and Theoretical Study," *Journal of Composites for Construction*, V. 24, No. 3, 2020, pp. 04020016.

5. Abdelazim, W.; Mohamed H. M.; Benmokrane, B.; and Nolan, S., "Strength of Bridge High-Strength Concrete Slender Compression Members Reinforced with GFRP Bars and Spirals: Experiments and Second-Order Analysis," *Journal of Bridge Engineering,* V. 25, No. 9, 2020, pp. 04020066.

6. Hasan, H. A.; Sheikh, M. N.;and Hadi, M. N., "Performance Evaluation of High Strength Concrete and Steel Fibre High Strength Concrete Columns Reinforced with GFRP Bars and Helices," *Construction and Building Materials,* V. 134, 2017, pp. 297-310.

7. Kharal, Z., and Sheikh, S. A., "Seismic Behavior of Square and Circular Concrete Columns with GFRP Reinforcement," *Journal of Composites for Construction,* V. 24, No. 1, 2020, pp. 04019059.

8. Hales, T. A.; Pantelides, C. P.; and Reaveley, L. D., "Experimental Evaluation of Slender High-Strength Concrete Columns with GFRP and Hybrid Reinforcement," *Journal of Composites for Construction,* V. 20, No. 6, 2016, pp. 04016050.

9. Guérin, M.; Mohamed, H. M.; Benmokrane, B.; Shield, C. K.; and Nanni, A., "Effect of Glass Fiber-Reinforced Polymer Reinforcement Ratio on Axial-Flexural Strength of Reinforced Concrete Columns," *ACI Structural Journal,* V. 155, No. 4, 2018, pp. 1049-1061.

10. Guérin, M.; Mohamed, H. M.; Benmokrane, B.; Nanni, A.; and Shield, C. K.,"Eccentric Behavior of Full-Scale Reinforced Concrete Columns with Glass Fiber-Reinforced Polymer Bars and Ties," *ACI Structural Journal,* V. 115, No. 2, 2018, pp. 489-499.

11. MacGregor, J. G., and Breen, J. E., "Design of Slender Concrete Columns," *Journal Proceedings,* V. 67, No. 1, 1970, pp. 6-28.

12. ACI 318 Committee, "Building Code Requirements for Structural Concrete (ACI 318-19)," American Concrete Institute, Farmington Hills, MI, 2019.

13. Mirmiran, A.; Yuan, W.; and Chen, X., "Design of Slenderness in Concrete Columns Internally Reinforced with Fiber-Reinforced Polymer Bars," *ACI Structural Journal,* V. 98, No. 1, 2001, pp. 116-125.

14. Zadeh, H. J., and Nanni, A., "Design of RC Columns Using Glass FRP Reinforcement," *Journal of Composites for Construction,* V. 17, No. 3, 2013, pp. 294-304.

15. Zadeh, H. J., and Nanni, A., "Flexural Stiffness and Second-Order Effects in Fiber-Reinforced Polymer-Reinforced Concrete Frames," *ACI Structural Journal,* V. 114, No. 2, 2017, pp. 533-543.

16. Abdelazim, W.; Mohamed, H. M.; Afifi, M. Z.; and Benmokrane, B., "Proposed Slenderness Limit for Glass Fiber-Reinforced Polymer-Reinforced Concrete Columns Based on Experiments and Buckling Analysis," *ACI Structural Journal,* V. 117, No. 1, 2020, pp. 241-254.

17. Rackwitz R., and Flessler, B., "Structural Reliability under Combined Random Load Sequences," *Computers & Structures,* V. 9, No. 5, 1978, pp. 489-494.

18. Nowak A. S., and Collins, K. R., Reliability of structures, McGraw-Hill, 2000.

19. Khorramian, K., "Short and Slender Concrete Columns Internally or Externally Reinforced with Longitudinal Fiber-Reinforced Polymer Composites," PhD Thesis, Dalhousie University, Halifax, NS, Canada, 2020.

20. Popovics, S., "A Numerical Approach to The Complete Stress-Strain Curve of Concrete," *Cement and Concrete Research,* V. 3, No. 5, 1973, pp. 583-599.

21. Khorramian, K., and Sadeghian, P., "Behavior of Slender GFRP Reinforced Concrete Columns," in *ASCE-SEI Structures Congress, American Society of Civil Engineers*, St. Louis, Missouri, USA, 2019.

22. Khorramian, K., and Sadeghian, P., "Strengthening of Slender Circular Concrete Columns with Longitudinal CFRP Laminates and Transverse GFRP Wraps," *CSCE Annual Conference*, Fredericton, NB, Canada, 2018.

23. Jiang T., and Teng, J. G., "Theoretical model for slender FRP-confined circular RC columns," *Construction and building materials,* V. 32, 2012, pp. 66-76.

24. Khorramian, K., and Sadeghian, P., "Slender RC Columns Strengthened with A Novel Hybrid Strengthening System of External Longitudinal and Transverse FRPs," *Journal of Structural Engineering*, 2021, pp. in-press.

25. Hadi, M. N., and Youssef, J., "Experimental investigation of GFRP-Reinforced and GFRP-Encased Square Concrete Specimens under Axial and Eccentric Load, and Four-Point Bending Test," *Journal of Composites for Construction,* V. 20, No. 5, 2016, pp. 04016020.

26. Elchalakani, M., and Ma, G.,"Tests of Glass Fibre Reinforced Polymer Rectangular Concrete Columns Subjected to Concentric and Eccentric Axial Loading," *Engineering Structures,* V. 151, 2017, pp. 93-104.

27. Khorramian, K., and Sadeghian, P., "Experimental and analytical behavior of short concrete columns reinforced with GFRP bars under eccentric loading," *Engineering Structures,* V. 151, 2017, pp. 761–773.

28. Sun, L.; Wei M.; and Zhang, N., "Experimental Study on The Behavior of GFRP Reinforced Concrete Columns under Eccentric Axial Load," *Construction and Building Materials,* V. 152, 2017, pp. 214-225.

29. Elchalakani, M.; Karrech, A.; Dong, M.; Ali M. M.; and Yang, B., "Experiments and Finite Element Analysis of GFRP Reinforced Geopolymer Concrete Rectangular Columns Subjected to Concentric and Eccentric Axial Loading," *Structures,* V. 14, 2018, pp. 273-289.

30. Xue, W.; Peng F.; and Fang, Z., "Behavior and Design of Slender Rectangular Concrete Columns Longitudinally Reinforced with Fiber-Reinforced Polymer Bars," *ACI Structural Journal,* V. 115, No. 2, 2018, pp. 311-322.

31. Salah-Eldin, A.; Mohamed H. M.; and Benmokrane, B., "Structural Performance of High-Strength-Concrete Columns Reinforced with GFRP Bars and Ties Subjected to Eccentric Loads," *Engineering Structures,* V. 185, 2019, pp. 286-300.

32. Elchalakani, M.; Dong, M.; Karrech, A.; Li, G.; Mohamed Ali, M. S.; and Yang, B., "Experimental Investigation of Rectangular Air-Cured Geopolymer Concrete Columns Reinforced with GFRP bars and Stirrups," *Journal of Composites for Construction,* V. 23, No. 3, 2019, pp. 04019011.

33. Salah-Eldin, A., Mohamed H. M.; and Benmokrane, B., "Effect of GFRP Reinforcement Ratio on the Strength and Effective Stiffness of High-Strength Concrete Columns: Experimental and Analytical Study," *Journal of Composites for Construction,* V. 24, No. 5, 2020, pp. 04020055.

34. Hognestad, E., "A Study of Combined Bending and Axial Load in Reinforced Concrete Members, Bulletin Series No. 399," University of Illinois, Urbana, 1951.

35. Kim, J.-K., and Yang, J.-K., "Buckling Behaviour of Slender High-Strength Concrete Columns," *Engineering Structures,* V. 17, No. 1, 1995, pp. 39-51.

36. Malakzadeh, K., and Daei, M., "Hybrid FORM-Sampling Simulation Method For Finding Design Point and Importance Vector in Structural Reliability," *Applied Soft Computing,* V. 92, 2020, pp. 106313.

37. Naderpour, H.; Poursaeidi O.; and Ahmadi, M., "Shear Resistance Prediction of Concrete Beams Reinforced by FRP Bars Using Artificial Neural Networks," *Measurement,* V. 308, 2018, pp. 299-308.

38. Raza, A.; Shah, S. A. R.; ul Haq, F.; Arshad, H.; Raza, S. S.; Farhan, M.; and Waseem, M., "Prediction of Axial Load-Carrying Capacity of GFRP-Reinforced Concrete Columns Through Artificial Neural Networks," *Structures,* V. 28, 2020, pp. 1557-1571.

39. Ahmad, A.; Elchalakani, M.; Elmesalami, N.; El Refai, A.; and Abed, F., "Reliability Analysis of Strength Models for Short-Concrete Columns under Concentric Loading with FRP Rebars Through Artificial Neural Network," *Journal of Building Engineering,* V. 42 , 2021, pp. 102497.

40. Nielsen, M. A., Neural Networks and Deep Learning, San Francisco, CA: Determination Press, 2015.

41. Shield, C. K.; Galambos, T. V.; and Gulbrandsen, P., "On the history and reliability of the flexural strength of FRP reinforced concrete members in ACI 440.1 R," *Special Publication,* V. 275, 2011, pp. 1-18.

42. Nowak, A. S., and Szerszen, M. M., "Calibration of Design Code for Buildings (ACI 318): Part 1 — Statistical Models for Resistance," *ACI Structural Journal,* V. 100, No. 3, 2003, pp. 377-382.

43. Hadhood, A.; Mohamed, H. M.; Benmokrane, B.; Nanni A.; and Shield, C. K., "Assessment of Design Guidelines of Concrete Columns Reinforced with Glass Fiber-Reinforced Polymer Bars," *ACI Structural Journal,* V. 116, No. 4, 2019, pp. 193-207.

44. Mirza, S. A.; Lee, P. M.; and Morgan, D. L., "ACI stability resistance factor for RC columns," *Journal of Structural Engineering,* V. 113, No. 9, 1987, pp. 1963-1976.

45. ACI 318 Committee, "Building Code Requirements for Structural Concrete (ACI 318-83)," *American Concrete Institute,* Farmington Hills, MI, 1983.

46. CSA A23.3-19, "Design of concrete structures," *Canadian standard association*, 2019.

47. Oudah, F.; El Naggar, M. H.; and Norlander, G., "Unified System Reliability Approach For Single and Group Pile Foundations–Theory and Resistance Factor Calibration," *Computers and Geotechnics,* V. 108, 2019, pp. 173-182.

48. Szerszen, M. M., and Nowak, A. S., "Calibration of Design Code for Buildings (ACI 318): Part 2-Reliability Analysis and Resistance Factors," *ACI Structural Journal,* V. 100, No. 3, 2003, pp. 383-391.

49. Khorramian, K.; Oudah, F.; and Sadeghian, P., "Reliability-Based Evaluation of the Stiffness Reduction Factor for Slender GFRP Reinforced Concrete Columns," *CSCE Annual Conference*, Virtual, STR181, 2021, pp. 1-8.

Table. 1. Computer-based database for the training of ANN

Parameter	GFRP-RC columns		Steel-RC columns	
	Value	cases	Value	cases
Width of cross-section (B)	254, 457 mm	2	254 mm	1
End moment ratio (M_1/M_2)	-1, -0.5, 0, +0.5, +1	5	-1, -0.5, 0, +0.5, +1	5
Rebar layout (RL)	Two or four sided	2	Two sided	1
Shape of cross-section (SC)	Rectangular (h/b = 0.75, 1, 1.25)	3	Square (h/b = 1)	1
Concrete strength (f_c)	20, 35, 50, 65 MPa	4	20, 35, 50, 65 MPa	4
Reinforcement depth ratio (γ)	0.6, 0.75, 0.9	3	0.6, 0.75, 0.9	3
Steel yield stress (f_y)	-	-	300, 400, 500 MPa	3
Strength of GFRP bars in tension (f_{ftu})	500, 700, 900 MPa	3	-	-
Strength of GFRP bars in compression (f_{fcu}/f_{ftu})	0.5, 0.75, 1	3	-	-
Reinforcement ratio (ρ)	1, 2, 4, 6, 8 %	5	1, 2, 4, 6, 8 %	5
Modulus of elasticity of GFRP (E_f)	40, 50, 60 GPa	3	-	-
Modulus of elasticity of steel (E_s)	-	-	200 GPa	1
Eccentricity ratio (e/h)	0.1, 0.2, 0.3, 0.4, 0.5, 1	6	0.1, 0.2, 0.3, 0.4, 0.5, 1	6
Slenderness ratio (λ)	14, 17, 20, 22, 24, 27, 30, 33, 37, 40	10	14, 17, 20, 22, 24, 27, 30, 33, 37, 40	10
Total cases	-	5,832,000	-	54,000

Note: 1 mm = 0.0394 in.; 1 MPa = 145.038 psi; 1 GPa = 145.038 ksi.

Table. 2. Distributions of random variables for reliability analysis

Type		Random variable	Bias	COV	Distribution	Reference
Material	Concrete	Concrete strength (f_c)	Eq. (9)	0.1	Normal	Nowak and Szerszen [42]
	Steel	Yield stress (f_y)	1.145	0.05	Normal	Nowak and Szerszen [42]
	GFRP	Tensile strength (f_{ftu})	1.15	0.07	Normal	Shield et al. [41]
		Compression strength (f_{fcu})	1	0.13	Lognormal	Khorramian et al. [49]
Geometry		Depth of compressive bars (d_c)	0.99	0.04	Normal	Shield et al. [41]
		Depth of tensile bars (d_t)	0.99	0.04	Normal	Shield et al. [41]
Loads		Dead load (D)	1.05	0.1	Normal	Nowak and Szerszen [42]
		Live load (L)	1	0.18	Normal	Nowak and Szerszen [42]
Modeling		FDM to experimental (ψ_{TE}) for GFRP-RC columns	1.1	0.14	Lognormal	Current study
		FDM to experimental (ψ_{TE}) for steel-RC columns	1.04	0.1	Lognormal	Current study

Note: COV = coefficient of variation.

Table. 3. Design space for the reliability analysis

Parameter	GFRP-RC columns			Steel-RC columns	
	Value	Cases	Reduced cases	Value	Cases
Width of cross-section (B)	254, 457 mm	2	1	254 mm	1
End moment ratio (M_1/M_2)	-1, -0.5, 0, +0.5, +1	5	5	-1, -0.5, 0, +0.5, +1	5
Rebar layout (RL)	Two or four sided	2	1	Two sided	1
Shape of cross-section (SC)	Rectangular (h/b = 0.75, 1, 1.25)	3	1	Square (h/b = 1)	1
Concrete strength (f_c)	20, 40, 60 MPa	3	3	20, 40, 60 MPa	3
Reinforcement depth ratio (γ)	0.6, 0.75, 0.9	3	3	0.6, 0.75, 0.9	3
Steel yield stress (f_y)	-	-	-	300, 400, 500 MPa	3
Strength of GFRP bars in tension (f_{ftu})	500, 700, 900 MPa	3	1	-	-
Strength of GFRP bars in compression (f_{fcu}/f_{ftu})	0.5, 0.75, 1	3	1	-	-
Reinforcement ratio (ρ)	1, 2, 4 %	3	3	1, 2, 4 %	3
Modulus of elasticity of GFRP (E_f)	40, 50, 60 GPa	3	3	-	-
Modulus of elasticity of steel (E_s)	-	-	-	200 GPa	1
Eccentricity ratio (e/h)	0.1, 0.3, 0.5	3	3	0.1, 0.3, 0.5	3
Slenderness ratio (λ)	14, 17, 20, 22, 24, 27, 30, 33, 37, 40	10	10	14, 17, 20, 22, 24, 27, 30, 33, 37, 40	10
Dead-to-live load ratio (D/L)	0.25,1, 2, 3, 4, 9, D=0, L=0	8	8	0.25,1, 2, 3, 4, 9, D=0, L=0	8
Total cases	-	10,497,600	97,200	-	97,200

Note: 1 mm = 0.0394 in.; 1 MPa = 145.038 psi; 1 GPa = 145.038 ksi.

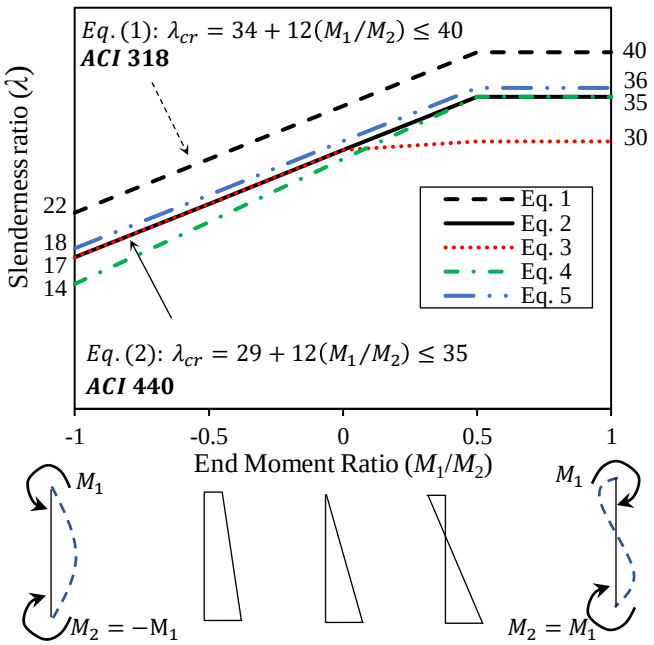

Fig. 1. Slenderness limit.

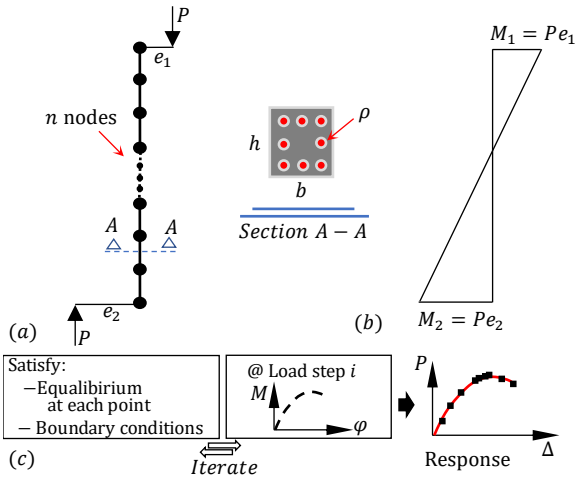

Fig. 2. Finite difference method (FDM): (a) schematic column; (b) moment diagram; and (c) analysis procedure.

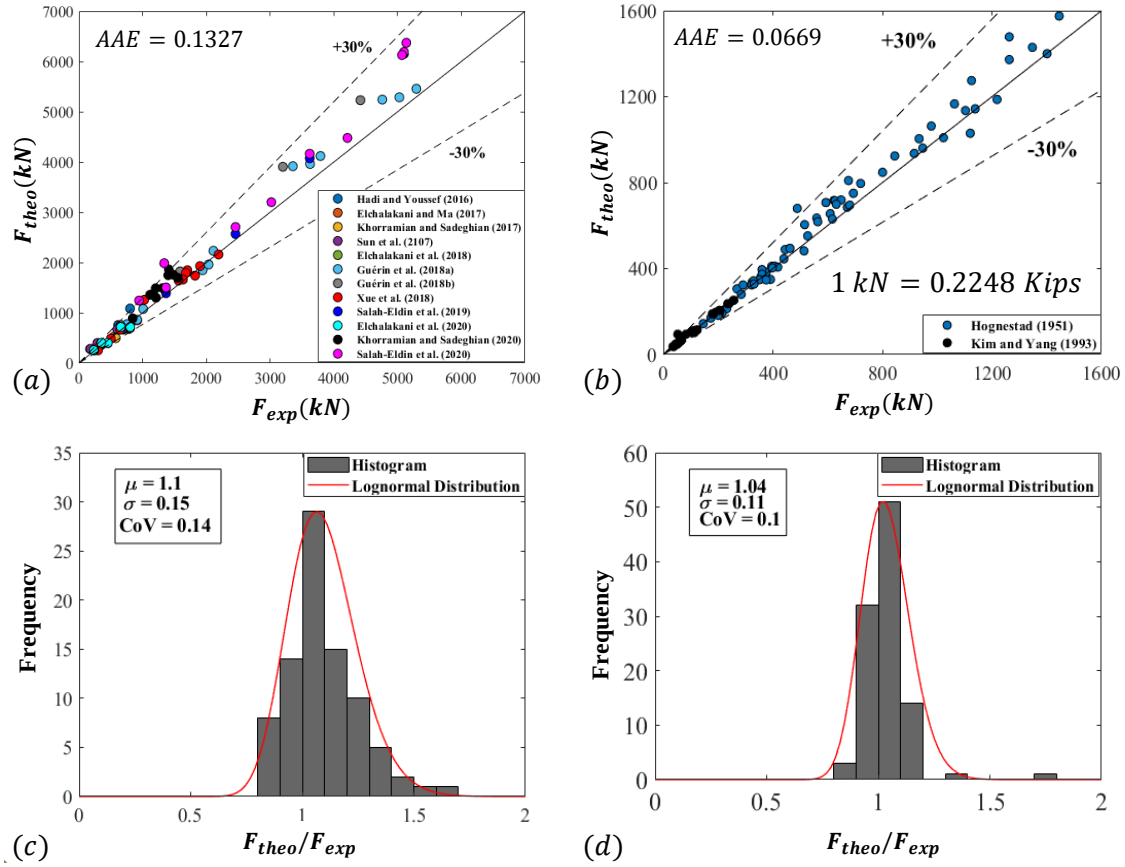

Fig. 3. Validation of FDM model: (a) FDM vs. experimental tests for GFRP-RC columns; (b) FDM vs. experimental tests for steel-RC columns; (c) histogram of the model to experimental data for GFRP-RC columns; and (d) histogram of the model to experimental data for steel-RC columns.

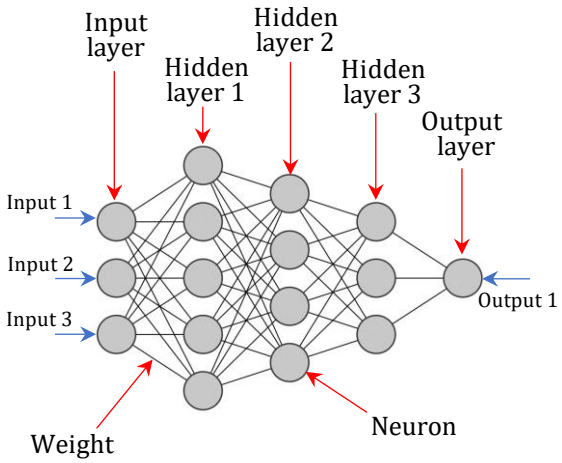

Fig. 4. Artificial neural network (ANN).

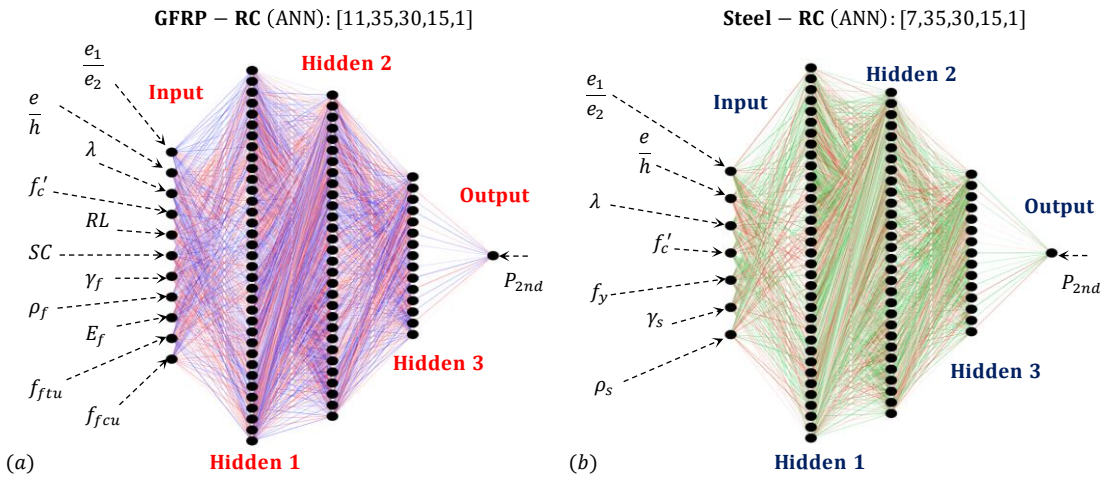

Fig. 5. Configuration of ANN analysis: (a) GFRP-RC columns and (b) steel-RC columns.

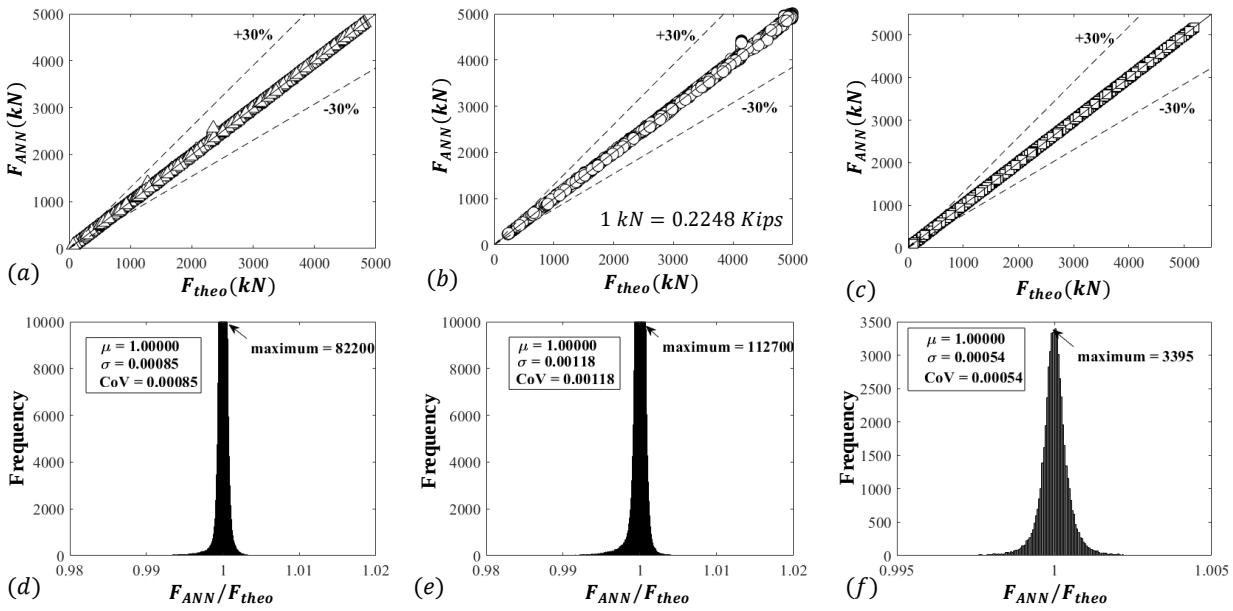

Fig. 6. Performance of the ANN model: (a) ANN vs. FDM for GFRP-R Columns with 254 mm width; (b) ANN vs. FDM for GFRP-RC columns with 457 mm width; (c) ANN vs. FDM for steel-RC columns with 254 mm width; (d) ANN/FDM histogram for GFRP-R Columns with 254 mm width; (e) ANN/FDM histogram for GFRP-RC columns with 457 mm width; and (f) ANN/FDM histogram for steel-RC columns with 254 mm width.

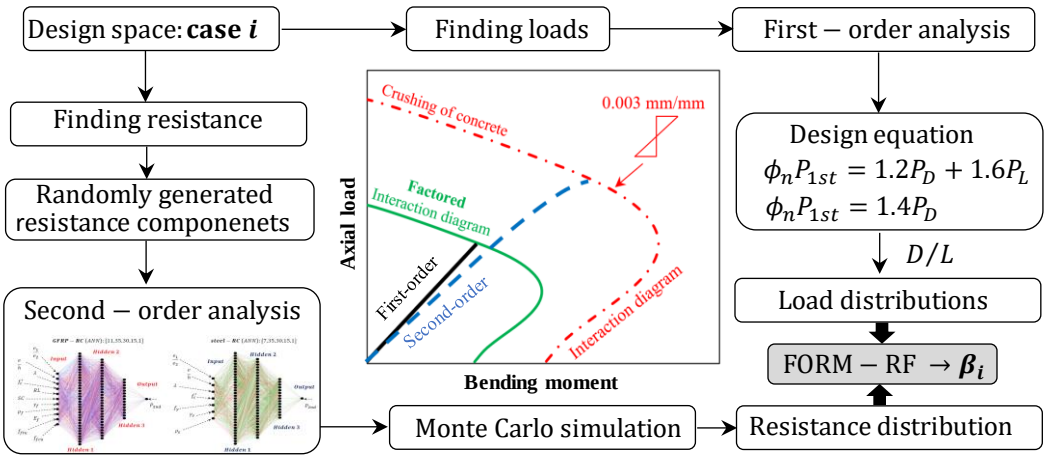

Fig. 7. Reliability analysis procedure.

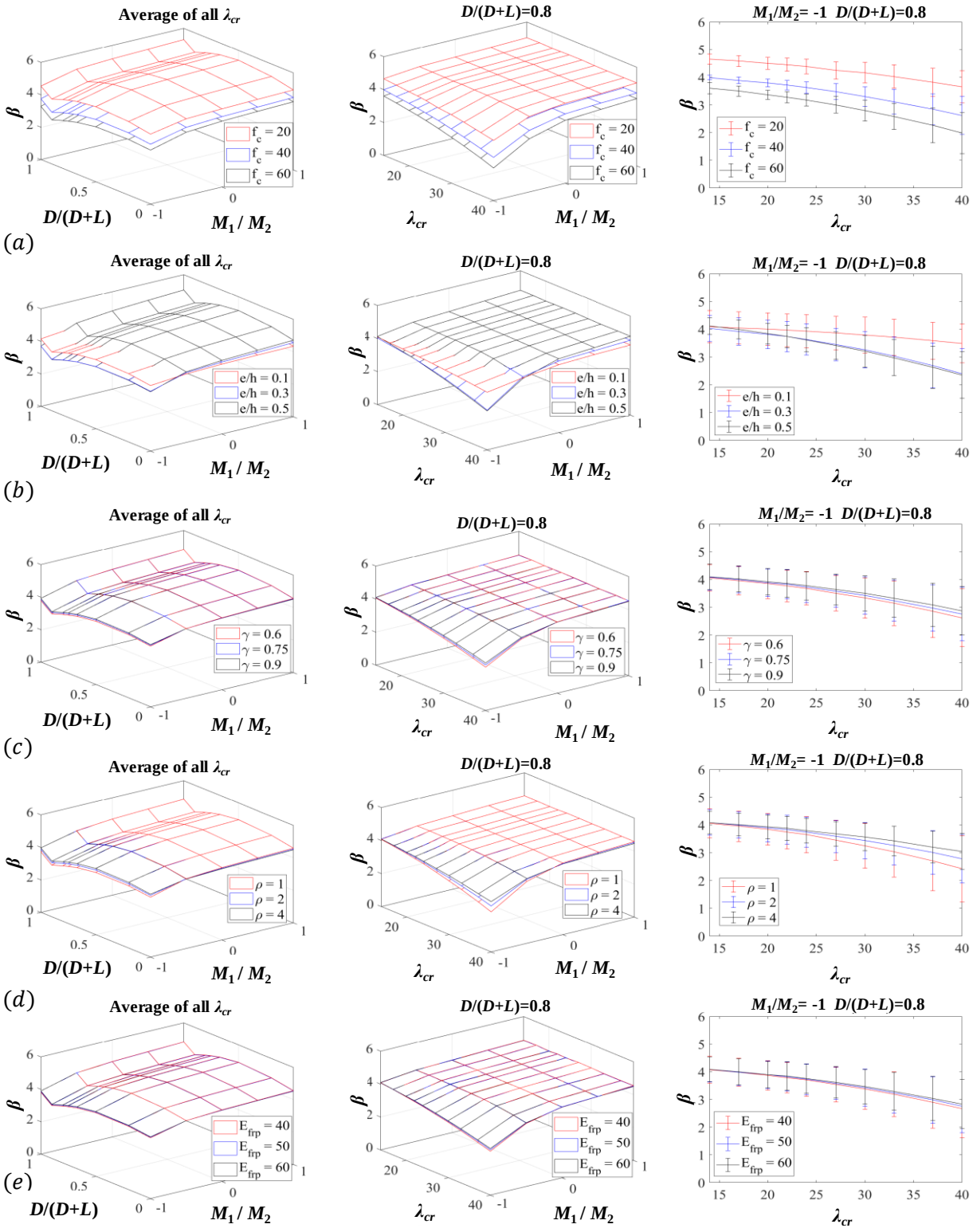

Fig. 8. Parametric study for GFRP-RC columns on the effect of: (a) concrete strength; (b) eccentricity ratio; (c) reinforcement depth ratio; (d) reinforcement ratio; and (e) modulus of elasticity of GFRP bars.

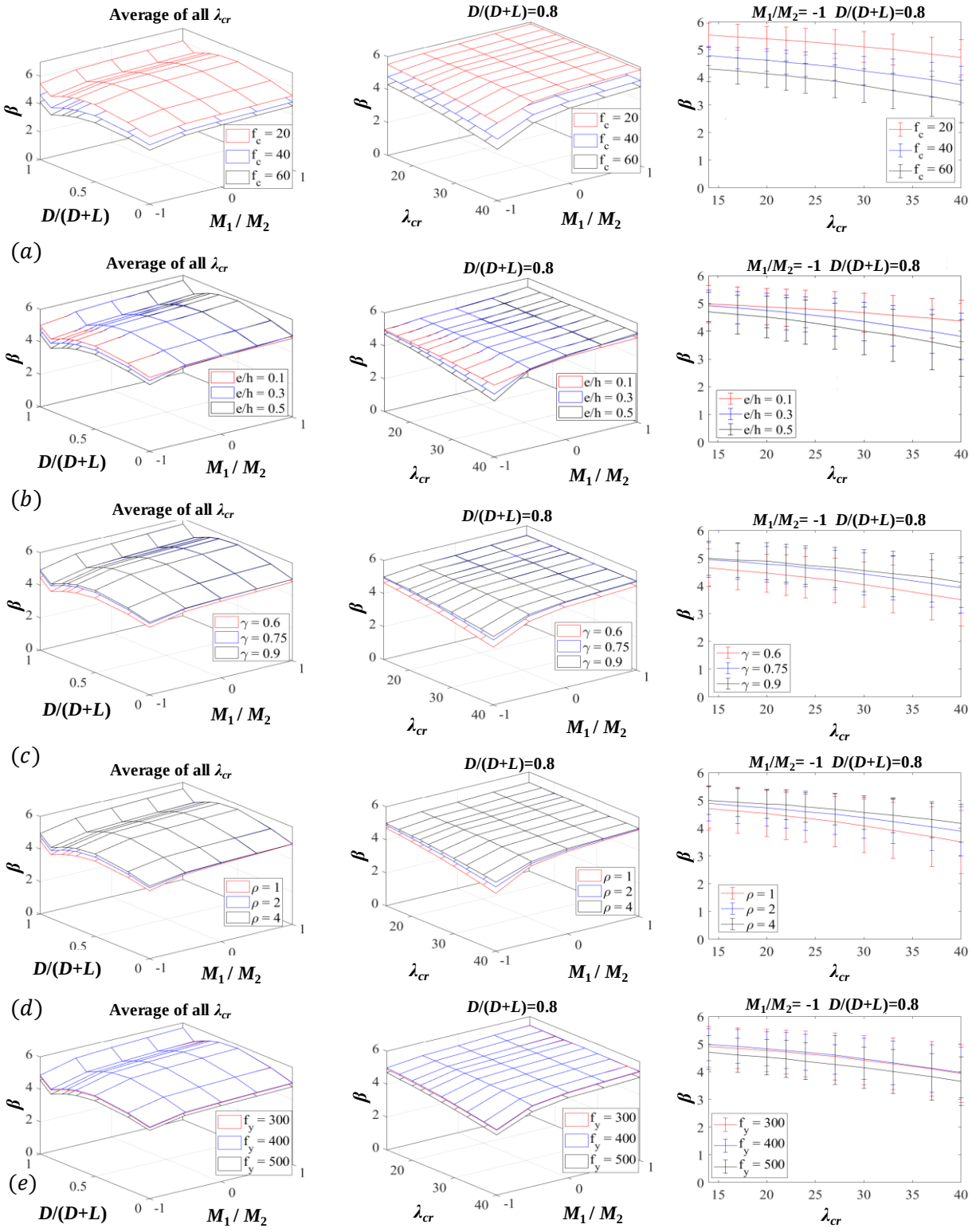

Fig. 9. Parametric study for steel-RC columns considering the effect of: (a) concrete strength; (b) eccentricity ratio; (c) reinforcement depth ratio; (d) reinforcement ratio; and (e) yield stress of steel rebar.

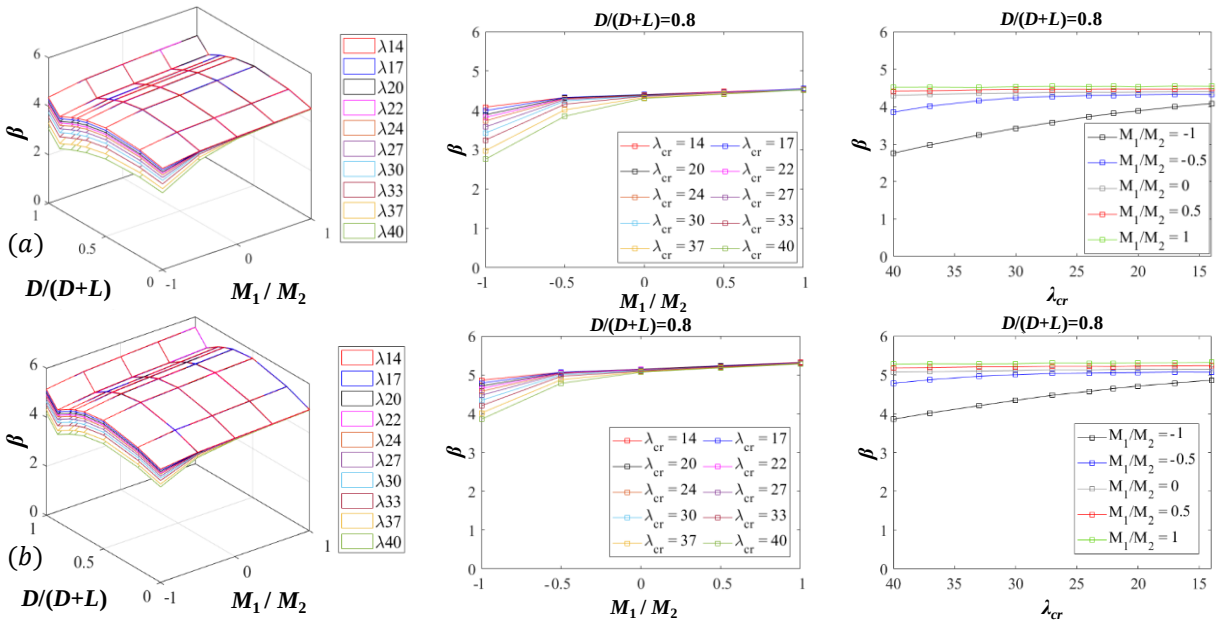

Fig. 10. Reliability analysis results for: (a) GFRP-RC columns; and (b) steel-RC columns.

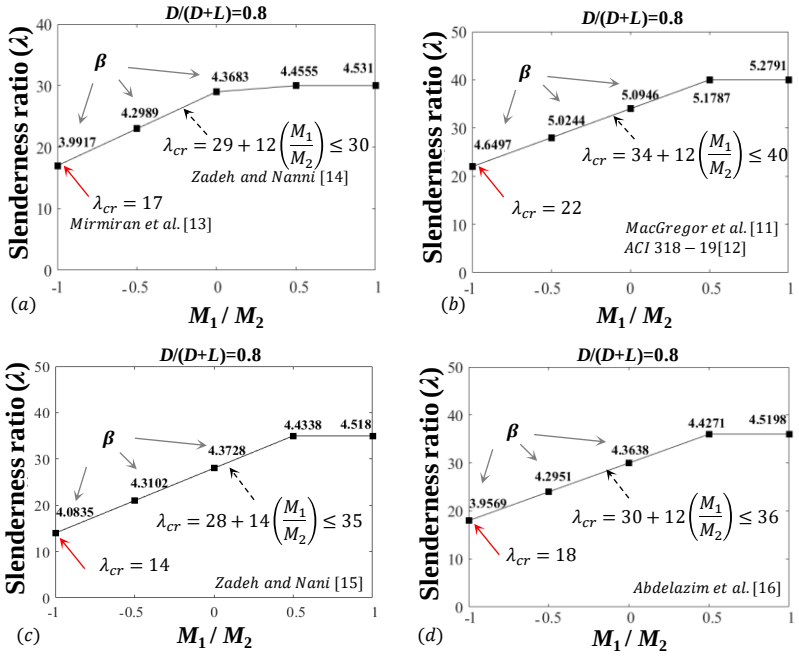

Fig. 11. Evaluation of the reliability indexes for slenderness limit: (a) ACI 440 code for GFRP-RC columns; (b) ACI 318-19 for steel-RC columns; (c) equation suggested by Zadeh and Nanni (2017) for GFRP-RC columns; and (d) equation suggested by Abdelazim et al. (2022) for GFRP-RC columns.

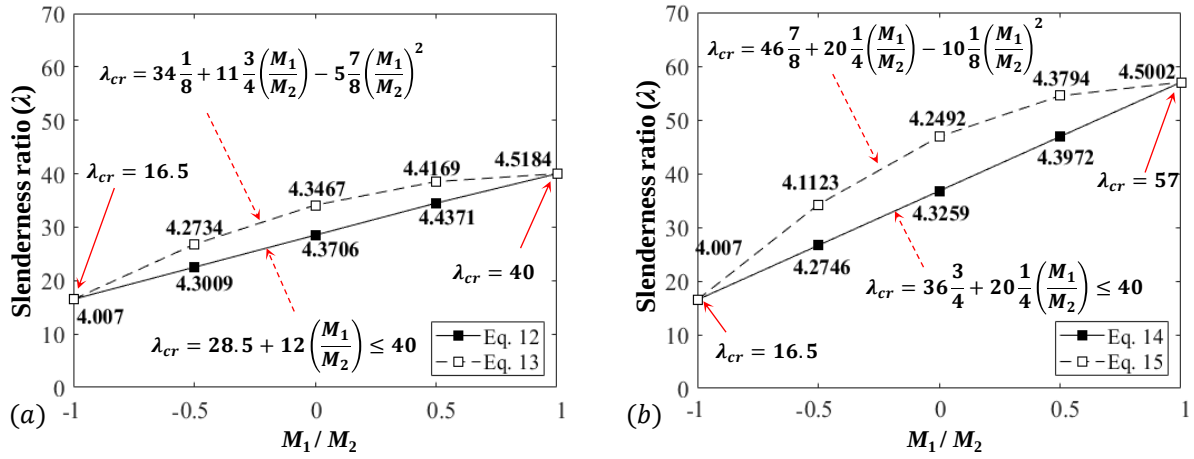

Fig. 12. Proposed slenderness limit for GFRP-RC columns (a) equations with a cap of 40 for slenderness limit and (b) equations without a cap for slenderness limit.

APPENDIX-1

This appendix presents Table. A1 which is the experimental database for eccentrically loaded GFRP-RC column tests in the literature.

Table. A1. Comparison of the FDM and the experimental database for GFRP-RC columns

No	Reference	Year	Specimen Label	f_c (MPa)	λ	e/h	F_{exp} (kN)	F_{theo} (kN)	F_{theo} / F_{exp}
1	Hadi and Youssef [25]	2016	RF-25	33.25	12.70	0.12	803	1085	1.35
2	Hadi and Youssef [25]	2016	RF-50	33.25	12.70	0.24	615	756	1.23
3	Elchalakani and Ma [26]	2017	G150-25	32.75	25.00	0.16	880.3	852	0.97
4	Elchalakani and Ma [26]	2017	G150-45	32.75	25.00	0.28	548.2	524	0.96
5	Elchalakani and Ma [26]	2017	G75-25	32.75	25.00	0.16	917.2	852	0.93
6	Elchalakani and Ma [26]	2017	G75-35	32.75	25.00	0.22	787.8	680	0.86
7	Khorramian and Sadeghian [27]	2017	R-e10-1	37	11.11	0.10	692.8	667	0.96
8	Khorramian and Sadeghian [27]	2017	R-e10-2	37	11.11	0.10	692.8	667	0.96
9	Khorramian and Sadeghian [27]	2017	R-e10-3	37	11.11	0.10	692.8	667	0.96
10	Khorramian and Sadeghian [27]	2017	R-e20-1	37	11.11	0.20	578.2	497	0.86
11	Khorramian and Sadeghian [27]	2017	R-e20-2	37	11.11	0.20	578.2	497	0.86
12	Khorramian and Sadeghian [27]	2017	R-e30-1	37	11.11	0.30	354.1	362	1.02
13	Khorramian and Sadeghian [27]	2017	R-e30-2	37	11.11	0.30	354.1	362	1.02
14	Sun et al. [28]	2017	Z175-1	33.51	13.33	0.70	201	281	1.40
15	Sun et al. [28]	2017	Z175-2	33.51	13.33	0.70	174	281	1.62
16	Sun et al. [28]	2017	Z175-3	33.51	13.33	0.70	181	281	1.56
17	Sun et al. [28]	2017	Z125-1	33.51	13.33	0.50	291	399	1.37
18	Sun et al. [28]	2017	Z125-2	33.51	13.33	0.50	290	399	1.38
19	Sun et al. [28]	2017	Z125-3	33.51	13.33	0.50	347	399	1.15
20	Sun et al. [28]	2017	Z75-1	33.51	13.33	0.30	632	671	1.06
21	Sun et al. [28]	2017	Z75-2	33.51	13.33	0.30	677	671	0.99
22	Sun et al. [28]	2017	Z75-3	33.51	13.33	0.30	602	671	1.11
23	Elchalakani et al. [29]	2018	G150-25	26	25.00	0.16	657	694	1.06
24	Elchalakani et al. [29]	2018	G75-25	26	25.00	0.16	804	694	0.86
25	Elchalakani et al. [29]	2018	G150-50	26	25.00	0.31	353	395	1.12
26	Elchalakani et al. [29]	2018	G75-50	26	25.00	0.31	454	395	0.87
27	Elchalakani et al. [29]	2018	G150-75	26	25.00	0.47	234	252	1.08
28	Elchalakani et al. [29]	2018	G75-75	26	25.00	0.47	244	252	1.03
29	Guérin et al. [9]	2018	G1e10	42.3	16.46	0.10	4760	5241	1.10
30	Guérin et al. [9]	2018	G1e20	42.3	16.46	0.20	3357	3916	1.17

31	Guérin et al. [9]	2018	G1e40	42.3	16.46	0.40	1942	1848	0.95
32	Guérin et al. [9]	2018	G1e80	42.3	16.46	0.79	754	773	1.02
33	Guérin et al. [9]	2018	G2e10	42.3	16.46	0.10	5028	5287	1.05
34	Guérin et al. [9]	2018	G2e20	42.3	16.46	0.20	3627	3961	1.09
35	Guérin et al. [9]	2018	G2e40	42.3	16.46	0.40	2035	1962	0.96
36	Guérin et al. [9]	2018	G2e80	42.3	16.46	0.79	914	862	0.94
37	Guérin et al. [9]	2018	G3e10	42.3	16.46	0.10	5294	5457	1.03
38	Guérin et al. [9]	2018	G3e20	42.3	16.46	0.20	3790	4119	1.09
39	Guérin et al. [9]	2018	G3e40	42.3	16.46	0.40	2110	2234	1.06
40	Guérin et al. [9]	2018	G3e80	42.3	16.46	0.79	1008	1077	1.07
41	Guérin et al. [10]	2018	CGB40	42.3	16.46	0.10	4417	5230	1.18
42	Guérin et al. [10]	2018	CGB80	42.3	16.46	0.20	3200	3905	1.22
43	Guérin et al. [10]	2018	CGB160	42.3	16.46	0.40	1589	1824	1.15
44	Guérin et al. [10]	2018	CGB320	42.3	16.46	0.79	654	754	1.15
45	Xue et al. [30]	2018	CE-1	39	20.00	0.20	1900	1929	1.02
46	Xue et al. [30]	2018	CE-2	39	20.00	0.50	647	664	1.03
47	Xue et al. [30]	2018	CE-3	39	20.00	1.00	306	305	1.00
48	Xue et al. [30]	2018	CE-4	39	26.67	0.20	1702	1846	1.08
49	Xue et al. [30]	2018	CE-5	40.3	33.33	0.20	1678	1792	1.07
50	Xue et al. [30]	2018	CE-6	40.3	40.00	0.20	1632	1662	1.02
51	Xue et al. [30]	2018	CE-7	40.3	40.00	0.50	500	485	0.97
52	Xue et al. [30]	2018	CE-8	40.3	40.00	1.00	300	252	0.84
53	Xue et al. [30]	2018	CE-9	40.3	40.00	0.20	1564	1641	1.05
54	Xue et al. [30]	2018	CE-10	40.3	40.00	0.20	1823	1739	0.95
55	Xue et al. [30]	2018	CE-11	29.1	40.00	0.20	1025	1259	1.23
56	Xue et al. [30]	2018	CE-12	55.2	40.00	0.20	2191	2160	0.99
57	Salah-Eldin et al. [31]	2019	Ge80	71.2	16.67	0.20	5100	6150	1.21
58	Salah-Eldin et al. [31]	2019	Ge120	71.2	16.67	0.30	3621	4074	1.13
59	Salah-Eldin et al. [31]	2019	Ge160	71.2	16.67	0.40	2457	2570	1.05
60	Salah-Eldin et al. [31]	2019	Ge240	71.2	16.67	0.60	1367	1389	1.02
61	Elchalakani et al. [32]	2019	G75-25	26.8	25.00	0.16	804	717	0.89
62	Elchalakani et al. [32]	2019	G75-50	26.8	25.00	0.31	454	403	0.89
63	Elchalakani et al. [32]	2019	G75-75	26.8	25.00	0.47	244	257	1.05
64	Elchalakani et al. [32]	2019	G150-25	26.8	25.00	0.16	657	717	1.09
65	Elchalakani et al. [32]	2019	G150-50	26.8	25.00	0.31	353	403	1.14
66	Elchalakani et al. [32]	2019	G150-75	26.8	25.00	0.47	234	257	1.10
67	Khorramian and Sadeghian [2]	2020	G17-e23-r4-N1	56.8	16.59	0.23	1401	1748	1.25
68	Khorramian and Sadeghian [2]	2020	G17-e23-r4-N2	56.8	16.59	0.23	1480	1758	1.19
69	Khorramian and Sadeghian [2]	2020	G22-e23-r4-N1	56.8	21.46	0.23	1550	1696	1.09
70	Khorramian and Sadeghian [2]	2020	G22-e21-r4-N2	56.8	21.46	0.21	1410	1862	1.32

71	Khorramian and Sadeghian [2]	2020	G40-e23-r2-N1	56.8	39.67	0.23	1210	1301	1.07
72	Khorramian and Sadeghian [2]	2020	G40-e23-r4-N2	56.8	39.67	0.23	1116	1358	1.22
73	Khorramian and Sadeghian [2]	2020	G40-e21-r2-N3	56.8	39.67	0.21	1204	1488	1.24
74	Khorramian and Sadeghian [2]	2020	G40-e21-r4-N4	56.8	39.67	0.21	1315	1491	1.13
75	Khorramian and Sadeghian [2]	2020	G60-e23-r4-N1	56.8	59.51	0.23	844	889	1.05
76	Salah-Eldin et al. [33]	2020	G1e80	71.2	16.67	0.20	5100	6188	1.21
77	Salah-Eldin et al. [33]	2020	G1e120	71.2	16.67	0.30	3621	4163	1.15
78	Salah-Eldin et al. [33]	2020	G1e160	71.2	16.67	0.40	2457	2706	1.10
79	Salah-Eldin et al. [33]	2020	G1e240	71.2	16.67	0.60	1367	1504	1.10
80	Salah-Eldin et al. [33]	2020	G2e80	71.2	16.67	0.20	5137	6371	1.24
81	Salah-Eldin et al. [33]	2020	G2e120	71.2	16.67	0.30	4213	4479	1.06
82	Salah-Eldin et al. [33]	2020	G2e160	71.2	16.67	0.40	3019	3200	1.06
83	Salah-Eldin et al. [33]	2020	G2e240	71.2	16.67	0.60	1338	1987	1.48
84	Salah-Eldin et al. [33]	2020	G3e80	71.2	16.67	0.20	5068	6128	1.21
85	Salah-Eldin et al. [33]	2020	G3e240	71.2	16.67	0.60	944	1243	1.32
Average									1.10
Standard deviation									0.15
Coefficient of variation									0.14

Note: F_{exp} = Axial load capacity determined from experimental tests; F_{theo} = Axial load capacity determined by the theoretical finite-difference modeling (FDM); *e/h* = eccentricity ratio; λ=slenderness ratio; f_c = concrete strength. The confinement effect is not considered in the modeling. Chamfers were neglected for the analysis. The effective length of the tests was considered as the total length of the columns; 1 kN = 0.2248 Kips; 1 MPa = 145.038 psi.

APPENDIX-2

This appendix presents Table. A2 which is the experimental database for eccentrically loaded steel-RC column tests in the literature. The references are limited to Hognestad [34] and Kim and Yang [35] because of the number and variety of the experimental tests in these studies (i.e., a range of 10.48 to 86.2 MPa for concrete strength, 10 to 100 for slenderness ratio, and 0.25 to 1.25 for eccentricity ratio) which make them comprehensive and sufficient to build a distribution of theoretical to experimental tests.

Table. A2. Comparison of the FDM and the experimental database for steel-RC columns

No	Reference	Year	Specimen Label	f_c (MPa)	λ	e/h	F_{exp} (kN)	F_{theo} (kN)	F_{theo} / F_{exp}
1	Hognestad [34]	1951	A-2a	36.4	25.67	0.25	1063.1	1166.5	1.10
2	Hognestad [34]	1951	A-2b	40.2	25.67	0.25	1125.4	1274.9	1.13
3	Hognestad [34]	1951	B-2a	29.3	25.67	0.25	947.5	960.6	1.01
4	Hognestad [34]	1951	B-2b	28.06	25.67	0.25	845.2	924.2	1.09
5	Hognestad [34]	1951	C-2a	15.65	25.67	0.25	527.1	552.4	1.05
6	Hognestad [34]	1951	C-2b	13.58	25.67	0.25	444.8	488.6	1.10
7	Hognestad [34]	1951	A-3a	39.02	25.67	0.50	593.8	707.4	1.19
8	Hognestad [34]	1951	A-3b	40.2	25.67	0.50	622.7	717.1	1.15
9	Hognestad [34]	1951	B-3a	31.92	25.67	0.50	560.0	635.1	1.13
10	Hognestad [34]	1951	B-3b	29.58	25.67	0.50	516.0	604.4	1.17
11	Hognestad [34]	1951	C-3a	12.96	25.67	0.50	269.1	305.7	1.14
12	Hognestad [34]	1951	C-3b	11.65	25.67	0.50	284.7	280.2	0.98
13	Hognestad [34]	1951	A-4a	33.16	25.67	0.75	375.9	383.4	1.02
14	Hognestad [34]	1951	A-4b	38.61	25.67	0.75	360.3	395.2	1.10
15	Hognestad [34]	1951	B-4a	26.2	25.67	0.75	355.9	360.7	1.01
16	Hognestad [34]	1951	B-4b	29.58	25.67	0.75	360.3	373.2	1.04
17	Hognestad [34]	1951	C-4a	11.65	25.67	0.75	223.3	208.8	0.93
18	Hognestad [34]	1951	C-4b	11.93	25.67	0.75	231.3	212.7	0.92
19	Hognestad [34]	1951	A-5a	33.16	25.67	1.25	214.4	192.8	0.90
20	Hognestad [34]	1951	A-5b	38.61	25.67	1.25	190.4	195.5	1.03
21	Hognestad [34]	1951	B-5a	29.58	25.67	1.25	205.1	190.5	0.93
22	Hognestad [34]	1951	B-5b	31.65	25.67	1.25	202.4	191.9	0.95
23	Hognestad [34]	1951	C-5a	15.93	25.67	1.25	173.5	169.5	0.98
24	Hognestad [34]	1951	C-5b	12.2	25.67	1.25	145.9	144.1	0.99
25	Hognestad [34]	1951	A-7a	37.37	25.67	0.33	1218.8	1186.9	0.97

26	Hognestad [34]	1951	A-7b	40.06	25.67	0.25	1263.3	1478.3	1.17
27	Hognestad [34]	1951	B-7a	28.13	25.67	0.25	1138.7	1143.4	1.00
28	Hognestad [34]	1951	B-7b	27.85	25.67	0.25	1103.2	1135.5	1.03
29	Hognestad [34]	1951	C-7a	13.58	25.67	0.25	627.2	715.8	1.14
30	Hognestad [34]	1951	C-7b	10.48	25.67	0.25	564.0	618.1	1.10
31	Hognestad [34]	1951	A-8a	38.06	25.67	0.50	720.6	796.2	1.10
32	Hognestad [34]	1951	A-8b	40.06	25.67	0.50	676.1	809.6	1.20
33	Hognestad [34]	1951	B-8a	32.41	25.67	0.50	693.9	750.3	1.08
34	Hognestad [34]	1951	B-8b	29.37	25.67	0.50	649.4	719.5	1.11
35	Hognestad [34]	1951	C-8a	12.55	25.67	0.50	440.4	445.3	1.01
36	Hognestad [34]	1951	C-8b	12.55	25.67	0.50	440.4	445.3	1.01
37	Hognestad [34]	1951	A-9a	35.16	25.67	0.75	395.9	410.6	1.04
38	Hognestad [34]	1951	A-9b	35.65	25.67	0.75	405.7	411.2	1.01
39	Hognestad [34]	1951	B-9a	32.41	25.67	0.75	418.1	406.8	0.97
40	Hognestad [34]	1951	B-9b	30.13	25.67	0.75	398.1	403.2	1.01
41	Hognestad [34]	1951	C-9a	12.96	25.67	0.75	324.7	337.5	1.04
42	Hognestad [34]	1951	C-9b	11.93	25.67	0.75	291.4	323.6	1.11
43	Hognestad [34]	1951	A-10a	35.16	25.67	1.25	205.1	198.1	0.97
44	Hognestad [34]	1951	A-10b	35.65	25.67	1.25	195.7	198.1	1.01
45	Hognestad [34]	1951	B-10a	29.37	25.67	1.25	193.5	196.0	1.01
46	Hognestad [34]	1951	B-10b	30.13	25.67	1.25	195.7	196.3	1.00
47	Hognestad [34]	1951	C-10a	15.86	25.67	1.25	197.9	187.2	0.95
48	Hognestad [34]	1951	C-10b	12.2	25.67	1.25	200.2	182.5	0.91
49	Hognestad [34]	1951	A-12a	28.61	25.67	0.25	1401.2	1400.0	1.00
50	Hognestad [34]	1951	A-12b	34.82	25.67	0.25	1445.7	1575.3	1.09
51	Hognestad [34]	1951	B-12a	29.65	25.67	0.25	1347.8	1429.4	1.06
52	Hognestad [34]	1951	B-12b	27.65	25.67	0.25	1263.3	1372.5	1.09
53	Hognestad [34]	1951	C-12a	15.86	25.67	0.25	1120.9	1029.6	0.92
54	Hognestad [34]	1951	C-12b	15.17	25.67	0.25	1023.1	1008.9	0.99
55	Hognestad [34]	1951	A-13a	36.89	25.67	0.50	978.6	1063.2	1.09
56	Hognestad [34]	1951	A-13b	33.44	25.67	0.50	934.1	1004.0	1.07
57	Hognestad [34]	1951	B-13a	24.68	25.67	0.50	800.7	847.9	1.06
58	Hognestad [34]	1951	B-13b	29.58	25.67	0.50	916.3	935.8	1.02
59	Hognestad [34]	1951	C-13a	15.86	25.67	0.50	671.7	685.4	1.02
60	Hognestad [34]	1951	C-13b	14.27	25.67	0.50	609.4	655.5	1.08
61	Hognestad [34]	1951	A-14a	36.89	25.67	0.75	631.6	699.1	1.11
62	Hognestad [34]	1951	A-14b	35.16	25.67	0.75	680.6	695.1	1.02
63	Hognestad [34]	1951	B-14a	37.09	25.67	0.75	617.4	630.9	1.02
64	Hognestad [34]	1951	B-14b	31.65	25.67	0.75	489.3	680.1	1.39
65	Hognestad [34]	1951	C-14a	13.44	25.67	0.75	513.8	482.5	0.94
66	Hognestad [34]	1951	C-14b	14.27	25.67	0.75	462.6	494.1	1.07
67	Hognestad [34]	1951	A-15a	35.16	25.67	1.25	391.4	349.6	0.89
68	Hognestad [34]	1951	A-15b	33.44	25.67	1.25	351.4	348.4	0.99

69	Hognestad [34]	1951	B-15a	26.2	25.67	1.25	329.2	342.8	1.04
70	Hognestad [34]	1951	B-15b	31.92	25.67	1.25	375.9	347.5	0.92
71	Hognestad [34]	1951	C-15a	13.44	25.67	1.25	322.5	324.0	1.00
72	Hognestad [34]	1951	C-15b	14.27	25.67	1.25	331.4	328.2	0.99
73	Kim and Yang [35]	1993	10L2-1	25.5	10	0.3	52.7	94.7	1.80
74	Kim and Yang [35]	1993	10L2-2	25.5	10	0.3	83.1	94.7	1.14
75	Kim and Yang [35]	1993	60L2-1	25.5	60	0.3	63.7	64.8	1.02
76	Kim and Yang [35]	1993	60L2-2	25.5	60	0.3	65.7	64.8	0.99
77	Kim and Yang [35]	1993	100L2-1	25.5	100	0.3	38.2	37.2	0.97
78	Kim and Yang [35]	1993	100L2-2	25.5	100	0.3	35.0	37.2	1.06
79	Kim and Yang [35]	1993	10M2-1	63.5	10	0.3	179.0	189.3	1.06
80	Kim and Yang [35]	1993	10M2-2	63.5	10	0.3	182.8	189.3	1.04
81	Kim and Yang [35]	1993	60M2-1	63.5	60	0.3	102.8	102.0	0.99
82	Kim and Yang [35]	1993	60M2-2	63.5	60	0.3	113.5	102.0	0.90
83	Kim and Yang [35]	1993	100M2-1	63.5	100	0.3	45.2	48.8	1.08
84	Kim and Yang [35]	1993	100M2-2	63.5	100	0.3	47.6	48.8	1.03
85	Kim and Yang [35]	1993	10H2-1	86.2	10	0.3	235.3	236.6	1.01
86	Kim and Yang [35]	1993	10H2-2	86.2	10	0.3	240.4	236.6	0.98
87	Kim and Yang [35]	1993	60H2-1	86.2	60	0.3	122.1	114.7	0.94
88	Kim and Yang [35]	1993	60H2-2	86.2	60	0.3	123.7	114.7	0.93
89	Kim and Yang [35]	1993	100H2-1	86.2	100	0.3	54.3	52.4	0.97
90	Kim and Yang [35]	1993	100H2-2	86.2	100	0.3	54.9	52.4	0.96
91	Kim and Yang [35]	1993	10L4-1	25.5	10	0.3	109.5	110.4	1.01
92	Kim and Yang [35]	1993	10L4-2	25.5	10	0.3	109.3	110.4	1.01
93	Kim and Yang [35]	1993	100L4-1	25.5	100	0.3	49.0	46.5	0.95
94	Kim and Yang [35]	1993	100L4-2	25.5	100	0.3	47.0	46.5	0.99
95	Kim and Yang [35]	1993	10M4-1	63.5	10	0.3	207.7	205.3	0.99
96	Kim and Yang [35]	1993	10M4-2	63.5	10	0.3	204.6	205.3	1.00
97	Kim and Yang [35]	1993	100M4-1	63.5	100	0.3	59.6	63.4	1.06
98	Kim and Yang [35]	1993	100M4-2	63.5	100	0.3	60.5	63.4	1.05
99	Kim and Yang [35]	1993	10H4-1	86.2	10	0.3	255.8	252.5	0.99
100	Kim and Yang [35]	1993	10H4-2	86.2	10	0.3	257.7	252.5	0.98
101	Kim and Yang [35]	1993	100H4-1	86.2	100	0.3	66.6	68.8	1.03
102	Kim and Yang [35]	1993	100H4-2	86.2	100	0.3	64.7	68.8	1.06
Average									1.04
Standard deviation									0.11
Coefficient of variation									0.10

Note: F_{exp} = Axial load capacity determined from experimental tests; F_{theo} = Axial load capacity determined by the theoretical finite-difference modeling (FDM); e/h = eccentricity ratio; λ=slenderness ratio; f_c = concrete strength. The confinement effect is not considered in the modeling. Chamfers were neglected for the analysis. The effective length of the tests was considered as the total length of the columns; 1 kN = 0.2248 Kips; 1 MPa = 145.038 psi.